Ethane Conversion to Ethylene In a Direct Hydrocarbon Fuel Cell

Matthew Wurtele

Thesis submitted to the
Faculty of Graduate and Postdoctoral Studies
In partial fulfillment of the requirements for the degree of

Master of Applied Science

In

Department of Chemical and Biological Engineering
Faculty of Engineering
UNIVERSITY OF OTTAWA

ABSTRACT

Direct hydrocarbon fuel cells are fuel cells than use hydrocarbons directly as fuel instead of the most commonly used fuel in a fuel cell, hydrogen. Studies are being done on direct hydrocarbon fuel cells because they have the potential to be energetically more efficient than hydrogen fuel cells. There are many different hydrocarbons that are available to use as a feed stock and each one reacts at different reaction rates. As the current density of a fuel cell is linked to the reaction rate, it is important to know the energetics of an oxidation reaction that is occurring.

Density Functional Theory (DFT) is a technique that can be used to predict the energy states of intermediate reaction steps in a given mechanism. The focus of this study is the using DFT to explore the energetics of the oxidation of ethane to ethylene in a nickel-anode catalyst fuel cell. DFT was used in adsorption runs to optimize the geometries beginning (adsorbed ethane) and end (adsorbed ethylene) of the oxidation reaction. DFT was then used to calculate the energy of transition states by varying bond lengths. It was determined the removal of the second hydrogen from the ethyl radical (C_2H_5) is the most energy intensive step and, thus, the rate limiting step.

Hydrogen, ethane, and ethylene were all explored in this study. The heats of adsorption varied from largest to smallest in the order of ethylene, hydrogen, and ethane. It was determined that the heat of adsorption of hydrogen is sufficient to meet the energy requirements for the dissociation reaction. This may help explain why hydrogen reacts so readily in fuel cells. Conversely, the heats of adsorption for the hydrocarbons did not meet the energy requirements for the dissociation reactions. This may help explain why ethane and ethylene react more slowly in a fuel cell as compared to hydrogen. Also, the oxidation of ethane to ethylene requires two large activation energies. These two additional activation energies may help explain why ethylene reacts more readily than ethane in a fuel cell.

STATEMENT OF CONTRIBUTIONS OF COLLABORATORS

I hereby declare that I am the sole author of this thesis. I have performed the mathematical modeling and data analysis, and I have written all of the chapters contained in this thesis.

My supervisors, Dr. Marten Ternan in the Department of Chemical and Biological Engineering and Dr. Alain St-Amant in the Department of Chemistry at the University of Ottawa have provided excellent collaboration and guidance throughout this research. They also contributed with essential editorial comments.

ACKNOWLEDGEMENTS

I would like to thank my MASc supervisor, Dr. Marten Ternan, for giving me the opportunity to learn and expand my knowledge in chemical engineering principles, specifically applied to fuel cell technologies. His expertise, guidance, and enthusiasm were paramount in the development of my understanding of fuel cell technologies and in the interpretation of results.

I would also like to thank my co-supervisor, Dr. Alain St-Amant, for assisting me with UNIX and in the use of the software application to perform Density Functional Theory. His knowledge was essential in troubleshooting problems in results as they arose.

TABLE OF CONTENTS

LIST OF FIGURES

CHAPTER 1

INTRODUCTION

1.1. Background and Motivation

A fuel cell is a device that converts chemical energy into electrical energy through electrochemical reactions. The electrochemical reaction occurs when a fuel such as hydrogen reacts with an oxidant such as oxygen in air [1]. Fuel cells are normally classified by their electrolyte. In proton exchange membrane fuel cells (PEMFC) the electrolyte is a membrane that is located between the anode and the cathode. Those three components are referred to as a membrane electrode assembly (MEA). Fuel cells operate by introducing fuel to the anode where it is oxidized. Protons from the anode diffuse through the electrolyte towards the cathode in response to a proton concentration gradient. Simultaneously electrons formed at the anode flow through an external circuit in response to an electrical potential gradient to meet the protons at the cathode. This causes an electrical current. As a result work can be performed, such as driving an external motor. The protons, electrons, and oxidizing agent (i.e., oxygen in air) combine at the cathode to produce water and complete the electrochemical reaction. This process is displayed in Figure 1.1.

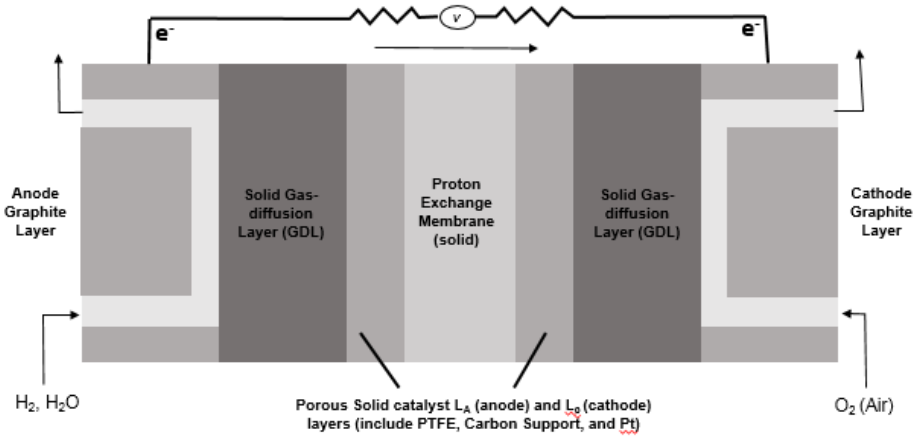

Figure 1-1: Cross section of a polymer electron membrane fuel cell with H_2 as the fuel supplied to the anode

The operating temperature is a factor that is associated with type of electrolyte used. The different fuel cell types that exist are: alkaline fuel cells (AFC, 45°C), solid oxide fuel cells (SOFC, 1000°C), molten carbonate fuel cells (MCFC, 600°C), phosphoric acid fuel cells (PAFC), and polymer electrolyte membrane fuel cells that are the most common form of proton exchange membrane fuel cells (PEMFC, 80°C) [2]. Fuel type is another classification factor. Commercially, hydrogen is the most common fuel, followed by methanol. There are fuel cells that employ other fuels such as ethanol, organic formates [3], organic hydrides [4], and hydrocarbons. Studies exist which employ these fuels in fuel cells [5]. Our research group focused on PEM fuel cells because they operate near ambient temperature and therefore can start-up rapidly.

Despite the discovery of hydrogen fuel cells in the early 19^{th} century, it was not until minimal environmental impact became important in the latter half of the 20^{th} century that hydrogen fuel cells were deemed to be an alternative energy generation technology. This was due to the inferior performance and greater cost of fuel cells in comparison to combustion engines and steam turbine systems. The very first fuel cell was limited by a low current density that was caused by the small effective area of platinum electrodes. Several years later fuel cells were developed that had a greater catalyst effective areas. These fuel cells generated power densities 50 times larger than the first one. Among the existing fuel cells, both the PEMFCs and the SOFCs have become commercially viable [6].

There are three categories of hydrogen fuel cells: stationary, portable and transport [7,8]. Since the late 1980s research into the use of PEMFCs in transportation has been significant. Studies exist which indicate that PEMFCs are viable alternatives to internal combustion engines due to their low operating temperatures that allow for quick start-ups and the possibility of zero emissions [6].

The rate of adoption of fuel cell technology in the year 2015 was reported [7], with the primary market being in the Asia Pacific. However, the gap between the North American, European and Asia Pacific markets is diminishing. The world's largest fuel cell plant was built in South Korea and operates at nearly 60 MW. A 360 MW fuel cell power plant in

Pyeongtaek City is expected to become operational in 2018 [9]. PEMFCs have been used commercially in fork-lifts, automotive vehicles, buses, and as back-up power. Other non-commercial applications of PEMFCs from a transport stance have been yachts, trains, and bicycles. Lifetimes for PEMFCs in applications related to transportation are approximately 2500 h. Their capital costs are $61/kW [10]. Major barriers for PEMFCs are durability (lifespan), cost, and sub-zero start-up.

In this work density functional theory (DFT) was used to study the reactions that occur when ethane and ethylene are the fuels used in a direct hydrocarbon fuel cell. DFT is a quantum mechanical theory that describes the ground state electronic structure of many-body systems. DFT allows for the properties of a many-electron system to be determined. DFT is one of the most versatile methods available to perform quantum mechanical calculations in condensed-matter physics, computational physics, and computational chemistry [11]. DFT studies have been performed to describe chemical reactions of ethane and ethylene on catalyst surfaces.

There were 7 chemical reactions on the surface of a nickel slab that were studied in this thesis:

$C_2H_6\ (g) \rightarrow C_2H_6\ (ads)$

$C_2H_6\ (ads) \rightarrow C_2H_5\ (ads) + H\ (ads)$

$C_2H_5\ (ads) \rightarrow C_2H_4\ (ads) + H\ (ads)$

$C_2H_4\ (ads) \rightarrow C_2H_4\ (g)$

$H_2\ (g) \rightarrow H_2\ (ads)$

$H_2\ (ads) \rightarrow 2\ H\ (ads)$

$H\ (ads) \rightarrow H\ (g)$

The electrochemical reaction in a PEM fuel cell is:

$H\ (ads) \rightarrow H^+ + e^-$

It is the only electrochemical reaction that occurs in hydrogen fuel cells and in hydrocarbon fuel cells. Since it is common to both types of fuel cells, it was not studied in this work. All of the other fuel cell reactions are chemical reactions.

The above chemical reactions were chosen in order to explore the energetics in each step of the oxidation of ethane to ethylene at the anode of the fuel cell. This oxidation reaction was chosen as it is the simplest hydrocarbon fuel having a C-C bond. In fuel cells and in steam reforming the reactions with hydrocarbons having two carbon atoms are much slower than those having one carbon atom. The literature shows that ethylene fuel cell reactions are faster than those of ethane. The purpose of this study was to examine the transition from ethane to ethylene in an attempt to understand why the ethane fuel cell performance is inferior to that of ethylene. The surface area of the nickel slab was chosen to be sufficiently large so that the adsorbed molecules would only interact with the nickel atoms. The adsorbed atom on one slab would be sufficiently far away from the adsorbed atom on neighboring slabs so that there would be no interactions between the adsorbed atoms or molecules.

1.2. References

[1] H. A. Liebhafsky & L. W. Niedrach, "Fuel cells"; *Journal of The Franklin Institute*; vol. 269; no. 4; pp. 257-267; 1960

[2] M. L. Perry & T. F. Fuller, "A historical perspective of fuel cell technology in the 20th century"; *Journal of The Electrochemical Society*; vol. 149; no. 7; pp. S59-S67, 2002

[3] Y. Li; "A liquid-electrolyte-free anion-exchange membrane direct formate-peroxide fuel cell"; *International Journal of Hydrogen Energy*; vol. 41; no. 5; pp. 3600-3604; 2016

[4] N. Kariya, A. Fukuoka, & M. Ichikawa; "Direct PEM fuel cell using 'organic chemical hydrides' with zero-CO2 emission and low-crossover"; *Physical Chemistry Chemical Physics*; vol. 8; no. 14; pp. 1724-1730; 2006

[5] T. G. Services; "*2004 fuel cell handbook: Advanced technology for generating electricity; series on renewable energy, Biofuels, Bioenergy, and Biobased products, 7th edition"*, 7th ed.; Morgantown, WV; U.S. Department of Energy, Office of Fossil Energy, National Energy Technology Laboratory; 2004

[6] G. J. K. Acres; "Recent advances in fuel cell technology and its applications"; *Journal of Power Sources*; vol. 100; no. 1-2; pp. 60-66; 2001

[7] K. A. Adamson; “The fuel cell and hydrogen: Annual review, 2016”; 4th Energy Wave; 2016

[8] Johnson Matthey PLC 2016; "Fuel cell applications"; 2016. [Online]; Available: http://www.fuelcelltoday.com/applications.

[9] T. Wilberforce, A. Alaswad, A. Palumbo, M. Dassisti, & A. G. Olabi; "Advances in stationary and portable fuel cell applications"; *International Journal of Hydrogen Energy*; vol. 41; no. 37; pp. 16509-16522; 2016

[10] Y. Wang, K. S. Chen, J. Mishler, S. C. Cho, & X. C. Adroher; "A review of polymer electrolyte membrane fuel cells: Technology, applications, and needs on fundamental research"; *Applied Energy*; vol. 88; no. 4; pp. 981-1007; 2011.

[11] D. Joubert; “Density Functionals: Theory and Application”, *Lecture Notes in Physics*, Springer-Verlog, Berlin, 1998

CHAPTER 2

LITERATURE REVIEW

2.1. An Overview of Fuel Cell Technology

A fuel cell is a device that converts energy through electrochemical reactions in order to convert chemical energy into electricity. The electrochemical reaction consists of a fuel such as hydrogen reacting with an oxidant such as oxygen in air [1]. The first fuel cell was invented in 1839 by William Grove and used hydrogen as the fuel source. This fuel cell was derived from a concept first postulated by Humphry Davy in 1801 [2]. Charles Langer and Ludwig Mond also performed fuel cell research using coal gas fuel and nickel catalysts [3].

Fuel cells are classified by the electrolyte (or membrane) that is used in the fuel cell. The operating temperature is the factor that decides which type of electrolyte is used. The different commercial fuel cell types that exist are: alkaline fuel cells (AFC), solid oxide fuel cells (SOFC), molten carbonate fuel cells (MCFC), phosphoric acid fuel cells (PAFC), and polymer electrolyte membrane fuel cells or proton exchange membrane fuel cells (PEMFC) [4]. Fuel type is another factor which can be used to classify fuel cells. Commercially, hydrogen is the most used fuel, followed by methanol in second place. There are fuel cells that employ other fuels such as ethanol, organic formates [5], organic hydrides [6], and hydrocarbons. Studies exist which employ these fuels in fuel cells [7].

Despite the discovery of hydrogen fuel cells in the early 19^{th} century, it was not until the latter half of the 20^{th} century that hydrogen fuel cells were deemed an alternative energy generation source with minimal environmental impact. This was due to the inferior performance of fuel cells in comparison to combustion engines and steam turbine systems. Grove's fuel cell

was limited by a low current density that was caused by the small effective surface area of platinum electrodes. Langer and Mond developed fuel cells that were more viable by using a catalyst with a higher effective surface area. These fuel cells generated power densities 50 times larger than Grove's model at the same voltage. Among the existing fuel cells, both the PEMFCs and the SOFCs have become commercially viable [8].

Fuel cells can be split into three main categories: stationary, portable and transport [11,12]. Since the late 1980s research into the use of PEMFCs in transportation has been significant. Studies exist which indicate that PEMFCs are viable alternatives to internal combustion engines due to low operating temperatures allowing for quick start-ups and the possibility of zero carbon dioxide emissions from a vehicle [8].

2.2. Direct Hydrocarbon Fuel Cells

From a theoretical perspective, direct hydrocarbon fuel cells (DHFC) could have a maximum electrical efficiency ($\Delta G/\Delta H$) of 95% [9]. The Carnot Cycle (used for internal combustion engines) has a maximum thermal efficiency ($\Delta G/\Delta H = [T_{OUT} - T_{IN}]/T_{IN}$) of 65%. Carnot Cycles are limited by the maximum operating temperatures, T_{IN}, of their construction materials (steel). As PEMFCs operate at lower temperatures, they do not have the same material limitations [10].

DHFCs work using the same principle as hydrogen fuel cells (HFC). The difference lies in the fuel used at the anode of the fuel cell. A redox reaction occurs that generates electrical energy from chemical energy. The membrane electrode assembly (MEA) located between the anode and the cathode in a PEM fuel cell consists of five layers: the anode gas diffusion layer, the anode catalyst layer, the electrolyte (or membrane) layer, the cathode catalyst layer, and the cathode gas diffusion layer [7].

As the fuel is fed to the anode, the fuel flows through the gas diffusion layer and through the catalyst layer. As the oxidant (oxygen in air) is fed to the cathode, the oxygen flows through

the cathode gas diffusion layer to the cathode catalyst layer. Protons (H+) are generated in the anode catalyst layer as the hydrocarbon reacts and flow through the electrolyte. Electrons (e-) are also generated at the anode and flow through an external circuit to the cathode catalyst layer. They combine at a three phase boundary (H+ in the electrolyte, e- in the solid metal cathode catalyst, and oxygen in the gas phase within the cathode catalyst layer) to form water. The flow of electrons through the external circuit is the source of electrical power.

Most studies in DHFCs employ alkane fuels like propane and methane. The existing hydrocarbon infrastructure and low cost of hydrocarbon production ~~is~~ the driving forces behind research into DHFCs. As hydrocarbons are directly fed into the fuel cells, costs associated with the steam reforming of alkanes into hydrogen can be eliminated. This has a potential of generating energy with ~~a~~ lower greenhouse gas (GHG) emissions because fuel cells have a greater energy efficiency [10].

2.3. Direct Hydrocarbon Fuel Cells with an Aqueous Electrolyte

DHFCs were studied most in the 1960s and 1970s. Reviews of these studies were made by Liebhafsky and Cairns [15], Bockris and Srinivasan [16], Bockris et al. [17], and Cairns [18]. Most studies during this period used an aqueous electrolyte. Numerous hydrocarbons (gasoline, diesel, hydrocarbons from methane to butane, and ethylene) were explored [10, 15, 38].

Previous studies indicate that DHFCs had a poor performance with current densities that fell below 20 mA/cm^2 at low cell potentials. Oswin et al. [19] investigated a direct propane fuel cell which had carbon-platinum electrodes and an electrolyte consisting of phosphoric acid in 1963. This study observed a good performance at an operating temperature of 160^oC and an electrolyte concentration of 85 wt% phosphoric acid.

Grubb and Michalske [20,21] studied several different hydrocarbon fuels including methane, propane, n-octane, and m-hexadecane in a fuel cell with an electrolyte consisting of 85 wt% phosphoric acid with electrodes that consisted of porous platinum. Normally methane has a

lower chemical reactivity in comparison to longer chain hydrocarbons. However, it was discovered that methane fuel could exceed propane in performance at operating temperatures above 150^{o}C. Similar to the work of Oswin et al., a good performance of the propane fuel cell was observed in the operating temperature range or 150^{o}C to 200^{o}C. Their fuel cell resulted in a near complete oxidation of propane, with a 99% yield of CO_2 product from propane.

One possible explanation for the high performance was a stronger adsorption of reaction intermediates on the platinum catalyst compared to the propane reactant. An increase in power density was observed as operating temperatures increased from 25^{o}C to 200^{o}C. A current density of 50 mA/cm^2 at a cell potential of 0.5 V was observed. Complete oxidation of propane was observed by Grubb using operating temperatures as low as 65^{o}C [22].

Studies by Cairns using DHFCs with an electrolyte consisting of an aqueous solution of CsF and HF salts at an operating temperature of 150^{o}C resulted in high performance when saturated short-chain hydrocarbons were used as a fuel source [23]. The hydrocarbon fuels were completely oxidized to CO_2 within an operating temperature range of 105^{o}C to 165^{o}C.

Other studies exist which use natural gas as a fuel source: Cairns in 1971 [18], Hsieh and Chen in 1977 [25], Murray et al. in 1999 [26], Lee et al. in 2013 [27], Lee et al. in 2016 [24], Baldinelli et al. in 2016 [28], and Choi et al. in 2016 [29]. Natural gas is often used as the fuel source as it is easily produced, stored, and transported. Natural gas infrastructure already exists.

2.4. Direct Hydrocarbon Polymer Electrolyte Membrane Fuel Cells

A direct propane fuel cell, DPFC, with an acid doped polybenzimidazole (PBI) electrolyte and operating temperature of 250^{o}C was used in a study by Cheng et al. [30]. Some blockage of reaction sites by an intermediate reactant was observed. This resulted in a low performance with current densities falling to 2 mA/cm^2 when water was not introduced with the fuel. After humidification, the performance improved to 15 mA/cm^2. It was noted that the open-circuit potential (OCP) remained constant at 0.7 V.

The use of carbonaceous fuels with an ion exchange membrane was explored in 1962 by Niedrach [31]. The fuel cell consisted of platinum or palladium based carbon electrodes in a sulfonated phenol-formaldehyde resin fuel cell. Methane, ethylene, propane, propylene, and carbon monoxide were used as fuel sources, but current densities seldom exceeded 5 mA/cm^2.

2.5. Direct Hydrocarbon Mixed Oxide Electrolyte Fuel Cell

In 2008, Heo et al. [38] performed studies on various hydrocarbon fuel sources using an operating temperature range of 100°C to 300°C with a membrane consisting of $Sn_{0.9}In_{0.1}$ P_2O_7 powder pressed into pellets. Catalysts in these studies were metal carbides supported on carbon. Current densities of 100 mA/cm^2 to 150 mA/cm^2 were observed with a 0.4 V cell potential. Various hydrocarbons (from methane to butane in chain length) were studied with platinum-free electrodes. A good performance was noted for propane and butane when operating conditions were 300°C with an anode electrode consisting of Mo_2C-ZrO_2/C. The open-circuit potential for both butane and propane was 0.8 V with a current density of 100 mA/cm^2 at 0.5 V.

2.6. Direct Hydrocarbon Solide Oxide Fuel Cell

In 2013, Lee et al. [27] investigated the performance of a SOFC fueled directly with methane using a $La_2Sn_2O_7$–Ni–GDC anode operating temperature above 600°C. The $La_2Sn_2O_7$ nanopowder increased the coking tolerance and the chemical stability of the Ni-based ceria anode catalyst for dry methane gas at 650°C. They also observed that the DMFC produced a peak power density of 0.94 W/cm^2 at 650°C.

Ding et al. [43] reported in 2016 on a high-performance direct methane SOFC which consisted of ceramic oxide electrodes and operating temperature between 550 and 700°C. The electrode material at the anode was synthesized by the reacting $SrCO_3$, iron (III) oxide, Fe_2O_3, Niobium (V) oxide, Nb_2O_5, and Molybdenum (VI) oxide, and MoO_3. The DMFC that consisted of a highly conductive anode layer and a cathode layer of $PrBaCo_2O_{5+\delta}$ generated a peak power density of 0.38 W/cm^2 at 0.85 V and 800°C. An open circuit potential of 0.81 V was observed at 800°C with a current density around 1.8 A/cm^2.

In 2016, Lee et al. [24] observed a high carbon monoxide tolerance in a direct methane solid oxide fuel cell with ceria coated Ni catalyst operating at 610°C. This fuel cell operated continuously for more than 1000 h at a steady current density of 1.2 A/cm^2 due to a reduction in coke deposition.

A direct butane SOFC was evaluated by Sumi et al. in 2012 [39]. They compared the performance of a SOFC employing nickel with gadolinia doped ceria (GDC) anode with the conventional nickel-yttria stabilized zirconia anode. A lower deposition rate of carbon on the catalyst surface was noted with the Ni-GDC anode compared to the Ni-YSZ anode. The coking effect on the anode catalyst surface was suppressed due to the reduction of ceria.

Liu et al. [40] investigated iso-octane as a fuel for a fuel cell intended for the transportation sector. They used an SOFC operating at 750°C with a double-layered anode designed to eliminate extensive coke deposition. The catalyst layer a layer of Ni-YSZ-BZY. It is used for the catalytic reforming of iso-octane when there is no hydrogen or carbon dioxide. The hydrogen produced from the reformation was passed through the porous electrochemical anode where the fuel was oxidized. This SOFC anode generated a peak power density of 0.6 W/cm^2.

Murray et al. [41] investigated a direct iso-octane SOFC with an operating temperature of 750°C in 2006. They evaluated the anode performance of the SOFC by feeding the fuel directly to the anode with a carrier nitrogen gas. The composition of the iso-octane in the carrier gas was 5.3% by volume. A peak power density of 0.34 W/cm^2 and an OCP of 1.078 V were noted with a limiting current density around 1 A/cm^2.

A SOFC directly fueled with dimethyl ether (DME) hydrocarbon fuel with an operating temperature range between 550 and 650°C was studied by Murray et al. 2005 [42]. A peak power density of 0.075 W/cm^2 at 650°C for both the anode fuels used (DME and DME (33%) + air mixture) and both performed with an OCP of 1 V.

In addition to hydrocarbon fuels, other fuels were also studied including: alcohols [44-45], formic acid [46], organic chemical hydrides [6], borohydride [47], and formate peroxide [5].

2.7. DFT Analysis of Electrochemical Reactions in Fuel Cells

Density functional theory (DFT) is a quantum mechanical theory that describes the ground state electronic structure of many-body systems. DFT allows for the properties of a many-electron system to be determined. DFT is one of the most versatile methods available to perform quantum mechanical calculations in condensed-matter physics, computational physics, and computational chemistry [48]. DFT studies have been performed to describe electrochemical reactions on catalyst surfaces and on the performance of electro-catalysts used in fuel cells.

Studies on the methanol electro-oxidation reaction at the anode were performed from 1998-2009 [49-50]. The purpose of the studies was to determine the rate limiting step and a mechanism for methanol electro-oxidation. DFT was used for calculating the energy barriers in all these studies. There are two main possible reaction mechanisms for the electro-oxidation of methanol to form CO [52].

Not all researchers agree upon the proposed mechanisms. From 1999 to 2008 numerous studies occurred where periodic DFT calculations were used to find a mechanism for methanol electro-oxidation on a catalyst surface. A consensus was reached and it was announced that stable adsorbed CO initially occurs through CO the initial C-H cleavage step to form an adsorbed hydroxymethyl species [53].

Zaragoza and Salcedo used DFT to demonstrate that the CH_3 fragment is the preferred chain end in both methanol and ethanol molecules during initial dehydrogenation [54].

In 2007 Janik et al. [55] proposed a different mechanism. They examined this reaction using pure platinum, pure ruthenium and different platinum-ruthenium alloys. DFT was used to calculate the energy barriers for all the intermediates [55]. The rate limiting step was determined

to be the reaction of adsorbed CH_2OH to form adsorbed CHOH step. This demonstrated that adsorbed carbon monoxide will react with adsorbed OH to form adsorbed COOH which will become CO_2 [55].

As governments have been subsidizing ethanol production from biomass, interest in direct ethanol fuel cells (DEFCs) has increased. The conversion of ethanol to CO_2 at the anode is what limits a DEFC's performance. Full oxidation of ethanol at the anode of DEFCs is difficult [56-57]. Ongoing research is being performed to find an optimal catalyst.

The ethanol oxidation reaction that occurs in fuel cells has been modelled using DFT. Wang and Liu [58] used SIESTA software. Kowal et al. [59] used the DMol3 code developed by Delley [60]. Wang and Liu investigated three Pt surfaces, Pt{100}, Pt{111}, and Pt{211}. They found that Pt{100} was the best surface to fully convert ethanol at low coverage. They concluded that C–C bond cleavage occurred through CH_2CO and CHCO intermediates. Kowal et al. used a $RuPt/SnO_2$ electrocatalyst. They claimed that this electrocatalyst could split the C–C at room temperature. Their DFT studies indicated that dehydrogenation of the CH_3 group and the OH group in CH_3CH_2OH occurred to form a CH_2CH_2O intermediate that reacted further to form two intermediates, CH_2 and CH_2O, thereby cleaving the C–C bond.

.

Galea et al. [61] proposed a mechanism for methane electro-oxidation at the anode in SOFC's in 2007. DFT was used to calculate the energy barriers. They concluded that adsorbed C will react with adsorbed O from the dissociation of water at the anode to produce adsorbed CO. This CO molecule then leaves the catalyst surfaces and enters the gas phase. CO (g) can then react with O_2 molecules transferred through the electrolyte [O^{2-} ions are transferred through a SOFC electrolyte not O_2 molecules] to produce CO_2 (g), water vapour, and electrons. The activation energy for each C-H bond breaking step was calculated and it was determined that the final methane C-H bond breaking step is rate limiting [62].

Psofogiannakis et al. [63] studied the methane electro-oxidation in PEM fuel cells using methane as a fuel source. Surface reactions in the mechanism included chemisorption of methane onto Pt, dehydrogenation of adsorbed intermediates, and oxygenation reactions of adsorbed

hydrocarbons. A mechanism for the electro-oxidation of propane in a DPFC was proposed as an extension of the mechanism proposed for methane [64]. Carbon monoxide is an intermediate ~~s~~ in the reaction mechanisms in both DMFC and DHFC. Carbon monoxide's strong adsorption on the surface of platinum poisons the Pt surface [65] even in trace amounts.

Janik and Neurock have done work on the CO oxidation reaction in DMFC [65]. They used DFT to calculate potential-dependent reaction energies and activation barriers. From this work a mechanism was proposed which includes hydroxylation of adsorbed CO and dehydrogenation of adsorbed COOH. The hydroxylation of adsorbed CO is rate limiting. This mechanism was confirmed by Ferrin et al. [66] and it was shown that this mechanism was favoured when Re, Ru, Os, Co or Ni was used as the anodic electro-catalyst. They employed DFT calculations with periodic boundary conditions.

Mukherjee and Linic performed a study on the H_2 electro-oxidation reaction on the surface of different metals at SOFC operating conditions [67]. It was proposed that hydrogen from the gas phase dissociates over two vacant sites on a metal surface, forming two adsorbed H atoms. Adsorbed oxygen is created through the transfer of oxygen anions through the electrolyte. The adsorbed H and adsorbed O react to form adsorbed OH. The adsorbed OH reacts with adsorbed H to form water.

Pacheco et al performed a study [68] on the Pt-H_2 interactions relevant to anode operation. It was demonstrated that initially physisorption of H_2 onto the Pt surface occurs, forming Pt-H_2. From here the H-H bond dissociates into two hydrogen atoms on the same platinum atom. The H-Pt-H complex has a bond angle of approximately 90 degrees. Energy calculations were performed using DFT on each step of this reaction.

Fuel cell research is being done in an attempt to discover an anodic electro-catalyst with a faster half-cell reaction that would have a higher current density and that would also have a high CO tolerance. A study [69] performed by Ferrin et al. evaluated a range of metals including Cu, Ag, Au (group IIB), Re, Ru, Os, Co, Rh, Ir, Ni, Pd and P. They discovered that group IIB metals had a good CO tolerance, but did not give the desired current densities. Platinum was the catalyst

that improved the densities the most. It was concluded that no single-element metal catalyst would solve these two issues.

Kua and Goddard performed a study on the anodic methanol reaction using 3rd row group VIII transition metals (Pt, Ir, Os, Pd, Rh, Ru) and one Pt-Ru alloy in 1999. Through their DFT calculations, platinum was deemed the only viable catalyst with Ir having notably better performance than the others transition metals. As Pt is susceptible to CO poisoning, a Pt-Ru alloy was tested along with Ru and Pt. Ru performed best in terms of barrier height and Pt performed worst. However the reaction caused by the Pt-Ru alloy was faster than both the pure metals. This is supported by their bifunctional roles where Pt is used for methanol dehydrogenation and Ru is used for water dissociation [70].

Christoffersen [71] performed a study of anode materials for low temperature fuel cells in 2001. They hypothesized that both H_2 and CO competed for the same reaction sites. Through testing many different metals and comparing the results to Pt, they concluded that the anode material must bind CO more weakly than pure Pt but still strong enough to perform the reaction with H_2. All Pt alloys with Ir, Rh, Ru, Cu, Ni, Co and Fe were deemed to meet these requirements.

Rossmeisl and Bessler [72] performed a study using periodic DFT calculations to determine the stability of adsorbed H, adsorbed O and adsorbed OH) on anodic electro-catalyst metals for use in SOFCs. It was found that although Ni had intermediate oxygen adsorption capabilities it still provides the fastest reaction speed.

Mukherjee and Linic performed a study of H_2 electro-oxidation at the anode in SOFCs [67] using numerous metals. A correlation was noted between the speed of the reaction and increasing anode potential. A trend was established in which the rate of electro-oxidation of hydrogen decreased when the oxygen atoms were bound too strongly or too weakly to the metal atoms [70].

In 2009 Kowal et al. [59] studied the effect of alloying on the performance of the electrocatalyst used in direct ethanol fuel cells, DEFC. A ternary electro-catalyst consisting of $PtRhSnO_2/C$ performed the complete electrooxidation of ethanol to CO_2. A comparison was made in the abilities of $PtRhSnO_2/C$, $PtSnO_2/C$, and $RhSnO_2/C$ to promote ethanol oxidation. It was demonstrated that $PtRhSnO_2$ caused C-C bond cleavage through a mechanism that has lower energy requirements during ethanol oxidation than the mechanism with $PtSnO_2$ or $RhSnO_2$ electrocatalysts.

The results were explained using the synergy between the three components of the alloy. SnO_2 strongly adsorbs water while interacting with Pt and Rh. SnO_2 also provides adsorbed OH to oxidize CO at free Rh sites. Pt and Rh interact strongly with the oxygen in ethanol for the ethanol oxidation reaction. A benefit of this is a weak interaction between Pt and ethanol and other oxygen-containing intermediates, thereby allowing Pt to more readily to assist in ethanol dehydrogenation. The presence of Pt modifies the electronic structure of Rh giving it more ability to adsorb both ethanol and other intermediates. This allows for faster C-C bond cleavage and a faster overall reaction.

Kelly et al. performed a study in 2011 on metal-modified tungsten carbide catalysts (M/WC). They wanted to find a mechanism for methanol oxidation in DMFC applications [73]. Their study indicated that Rh, Ni, and Pt were all catalysts that were able to facilitate methanol oxidation.

The capabilities of M/WC catalysts were also studied by Esposito and Chen [74] as a potential anode catalyst in DMFC through further modification of the catalysts. They used tungsten carbide with Pt in the top monolayer and hypothesized that the monolayer of Pt would yield catalytic properties closer to Pt than to tungsten carbide. Through a combination of both experiments and DFT, two challenges associated with DMFC were highlighted: the high cost of the catalyst, and Pt poisoning by CO. The modified catalyst can be a lower-cost alternative to bulk Pt at DMFC operating conditions, CO adsorbs more weakly on tungsten carbide and on the monolayer. This facilitates CO oxidation by the production of OH to react with CO to make CO_2.

This had the benefit of exposing more vacant reaction sites, making the catalyst both more cost-effective and faster-working, resulting in higher current densities.

Nikolla et al. used DFT to calculate whether or not a Sn-Ni alloy was more resistant to carbon poising in the steam reformation of hydrocarbons [75] than pure Ni used as the conventional catalyst. Through DFT they discovered that a Sn-Ni alloy has a better tolerance to carbon poisoning and was a better catalyst for oxidizing carbon atoms than creating C-C bonds.

Vukmirovic et al. [76] and Norskov et al. [77] both studied the effect of the catalyst on the oxygen reaction at the cathode. They tested electro-catalysts that were composed of either Pt or a Pt-alloy monolayer on the surface of either Pd single crystals or Pd-nanoparticles supported on carbon. The addition of Pd was found to increase the rate of reaction by a factor of 20. This is attributed to reduced Pt-OH coverage. By using a volcano plot ~~of~~ that included a number of transition metals it was determined that Pt and Pd stand out as the two metals with the smallest overpotential. This is attributed to the other transition metals being able to interact more strongly with oxygen and being poorer at reducing oxygen.

2.8. References

[1] H. A. Liebhafsky & L. W. Niedrach; "Fuel cells"; *Journal of The Franklin Institute*; vol. 269; no. 4; pp. 257-267; 1960

[] M. L. Perry and T. F. Fuller; "A historical perspective of fuel cell technology in the 20th century"; *Journal of The Electrochemical Society*; vol. 149; no. 7; pp. S59-S67; 2002

[5] Y. Li, "A liquid-electrolyte-free anion-exchange membrane direct formate-peroxide fuel cell," *International Journal of Hydrogen Energy*, vol. 41, no. 5, pp. 3600-3604; 2016

[6] N. Kariya, A. Fukuoka, and M. Ichikawa, "Direct PEM fuel cell using 'organic chemical hydrides' with zero-CO_2 emission and low-crossover," *Physical Chemistry Chemical Physics*, vol. 8, no. 14, pp. 1724-1730; 2006

[7] T. G. Services, *'2004 fuel cell handbook: Advanced technology for generating electricity; series on renewable energy, Biofuels, Bioenergy, and Biobased products, 7th edition'*, 7th ed. Morgantown, WV: U.S. Department of Energy, Office of Fossil Energy, National Energy Technology Laboratory; 2004

[8] G. J. K. Acres, "Recent advances in fuel cell technology and its applications," *Journal of Power Sources*, vol. 100, no. 1-2, pp. 60-66; 2001

[9] M. Ternan, “The potential of direct hydrocarbon fuel cells for improving energy efficiency,” *2006 IEEE EIC Climate Change Conference*, vol. 1-2, pp. 504-507; 2006

[10] G. Hoogers, “Introduction,” in *Fuel Cell Technology Handbook,* CRC Press, Boca Raton, pp. 2-37; 2003

[11] K. A. Adamson, “The fuel cell and hydrogen: Annual review, 2016,” 4th Energy Wave; 2016

[12] Johnson Matthey PLC 2016, "Fuel cell applications,"[Online]. Available: http://www.fuelcelltoday.com/applications; 2016

[13] Y. Wang, K. S. Chen, J. Mishler, S. C. Cho, and X. C. Adroher, "A review of polymer electrolyte membrane fuel cells: Technology, applications, and needs on fundamental research," *Applied Energy*, vol. 88, no. 4, pp. 981-1007; 2011.

[14] T. Wilberforce, A. Alaswad, A. Palumbo, M. Dassisti, and A. G. Olabi, "Advances in stationary and portable fuel cell applications," *International Journal of Hydrogen Energy*, vol. 41, no. 37, pp. 16509-16522; 2016

[15] H. A. Liebhafsky and E. J. Cairns, “Direct hydrocarbon fuel cell with aqueous electrolytes,” in *Fuel Cells and Fuel Batteries*, Wiley, New York, pp. 458-523; 1968

[16] J. O. Bockris and S. Srinivasan, “Fuel cells: Their electrochemistry,” in *ElectrochemicalCombustion of Organic Substances*, McGraw-Hill, New York, pp. 357-411; 1969

[17] J. O. Bockris, E. Gileadi, and G. E. Stoner, "Anodic oxidation of saturated hydrocarbons. Mechanistic study," *The Journal of Physical Chemistry*, vol. 73, no. 2, pp. 427-434; 1969

[18] E. J. Cairns, "The anodic oxidation of hydrocarbons and the hydrocarbon fuel cell," in *Advances in Electrochemistry and Electrochemical Engineering*, Wiley-Interscience, New York, vol. 8, pp. 337-392; 1972

[19] H. G. Oswin, A. J. Hartner, and F. Malaspina, "A direct hydrocarbon/air fuel cell," *Nature*, vol. 200, no. 4903, pp. 256-257; 1963

[20] W. T. Grubb and C. J. Michalske, "Electrochemical oxidation of methane in phosphoric acid fuel cells at 150°C," *Nature*, vol. 201, no. 4916, pp. 287-28; 1964

[21] W. T. Grubb and C. J. Michalske, "A high performance propane fuel cell operating in the temperature range of 150°C-200°C," *Journal of The Electrochemical Society*, vol. 111, no. 9, pp. 1015-1019; 1964

[22] W. T. Grubb, "Catalysis, electrocatalysis, and hydrocarbon fuel cells," *Nature*, vol. 198, no. 4883, pp. 883-884; 1963

[23] E. J. Cairns, "Hydrocarbon fuel cells with fluoride electrolytes," *Journal of The Electrochemical Society*, vol. 113, no. 11, pp. 1200-1204; 1966

[24] J. G. Lee, O. S. Jeon, H. J. Hwang, J. Jang, Y. Lee, S. H. Hyun, and Y. G. Shul, "Durable and high-performance direct-methane fuel cells with coke-tolerant ceria-coated Ni catalysts at reduced temperatures," *Electrochimica Acta*, vol. 191, pp. 677-686; 2016

[25] S. Y. Hsieh and K. M. Chen, "Anodic oxidation of methane," *Journal of The Electrochemical Society*, vol. 124, no. 8, pp. 1171-1174; 1977

[26] E. P. Murray, T. Tsai, and S. A. Barnett, "A direct-methane fuel cell with a ceria-based anode," *Nature*, vol. 400, no. 6745, pp. 649-651; 1999

[27] J. G. Lee, C. M. Lee, M. Park, and Y. G. Shul, "Direct methane fuel cell with La2Sn2O7–Ni–Gd0.1Ce0.9O1.95 anode and electrospun La0.6Sr0.4Co0.2Fe0.8O3−δ–Gd0.1Ce0.9O1.95 cathode," *RSC Advances*, vol. 3, no. 29, pp. 11816-11822; 2013

[28] A. Baldinelli, L. Barelli, G. Bidini, A. Di Michele, and R. Vivani, "SOFC direct fuelling with high-methane gases: Optimal strategies for fuel dilution and upgrade to avoid quick degradation," *Energy Conversion and Management*, vol. 124, pp. 492-503; 2016

[29] Y. Choi, E. C. Brown, S. M. Haile, and W. Jung, "Electrochemically modified, robust solid oxide fuel cell anode for direct-hydrocarbon utilization," *Nano Energy*, vol. 23, pp. 161-171; 2016

[30] C. K. Cheng, J. L. Luo, K. T. Chuang, and A. R. Sanger, "Propane fuel cells using phosphoric-acid-doped polybenzimidazole membranes." *The Journal of Physical Chemistry B*, vol. 109, no. 26, pp. 13036-13042; 2005

[31] L. W. Niedrach, "The performance of hydrocarbons in ion exchange membrane fuel cells," *Journal of The Electrochemical Society*, vol. 109, no. 11, pp. 1092-1096; 1962

[32] O. Savadogo and F. J. Rodriguez Varela, "Low-temperature direct propane polymer electrolyte membranes fuel cell (DPFC)," *Journal of New Materials for Electrochemical Systems*, vol. 4, no. 2, pp. 93-97; 2001

[33] F. J. Rodriguez Varela and O. Savadogo, "The effect of anode catalysts on the behavior of low temperature direct propane polymer electrolyte fuel cells (DPFC)," *Journal of New Materials for Electrochemical Systems*, vol. 9, no. 2, pp. 127-137; 2006

[34] A. Al-Othman, A. Y. Tremblay, W. Pell, S. Letaief, T. J. Burchell, B. A. Peppley, and M. Ternan, "Zirconium phosphate as the proton conducting material in direct hydrocarbon polymer electrolyte membrane fuel cells operating above the boiling point of water," *Journal of Power Sources*, vol. 195, no. 9, pp. 2520-2525; 2010

[35] F. N. Büchi and S. Srinivasan, "Operating proton exchange membrane fuel cells without external humidification of the reactant gases fundamental aspects," *Journal of the Electrochemical Society*, vol. 144, no. 8, pp. 2767-2772; 1997

[36] K. Ramya, J. Sreenivas, and K. S. Dhathathreyan, "Study of a porous membrane humidification method in polymer electrolyte fuel cells," *International Journal of Hydrogen Energy*, vol. 36, no. 22, pp. 14866-14872; 2011

[37] D. G. Sanchez, T. Ruiu, K. A. Friedrich, J. Sanchez-Monreal, and M. Vera, "Analysis of the influence of temperature and gas humidity on the performance stability of polymer electrolyte membrane fuel cells," *Journal of The Electrochemical Society*, vol. 163, no. 3, pp. F150-F159; 2016

[38] P. Heo, K. Ito, A. Tomita, and T. Hibino, "A proton-conducting fuel cell operating with hydrocarbon fuels," *Angewandte Chemie International Edition*, vol. 47, no. 41, pp. 7841-7844; 2008

[39] H. Sumi, T. Yamaguchi, K. Hamamoto, T. Suzuki, and Y. Fujishiro, "Impact of direct butane microtubular solid oxide fuel cells," *Journal of Power Sources*, vol. 220, pp. 74-78; 2012

[40] M. Liu, Y. Choi, L. Yang, K. Blinn, W. Qin, and P. Liu, "Direct octane fuel cells: A promising power for transportation," *Nano Energy*, vol. 1, no. 3, pp. 448-455; 2012

[41] E. P. Murray, S. J. Harris, J. Liu, and S. A. Barnett, "Direct solid oxide fuel cell operation using isooctane," *Electrochemical and Solid-State Letters*, vol. 9, no. 6, pp. A292–A294; 2006

[42] E. P. Murray, S. J. Harris, J. Liu, and S. A. Barnett, "Direct solid oxide fuel cell operation using a dimethyl ether/air fuel mixture," *Electrochemical and Solid-State Letters*, vol. 8, no.10, pp. A531-A533; 2005

[43] H. Ding, Z. Tao, S. Liu, and Y. Yang, "A redox-stable direct-methane solid oxide fuel cell (SOFC) with Sr2FeNb0.2Mo0.8O6−δ double perovskite as anode material," *Journal of Power Sources*, vol. 327, pp. 573-579; 2016

[44] J. Qi, N. Benipal, C. Liang, and W. Li, "PdAg/CNT catalyzed alcohol oxidation reaction for high-performance anion exchange membrane direct alcohol fuel cell (alcohol=methanol, ethanol, ethylene glycol and glycerol)," *Applied Catalysis B: Environmental*, vol. 199, pp. 494-503; 2016

[45] S. Fan, D. P. Wilkinson, and H. Wang, "Performance of the vapor fed direct alcohol phosphoric acid fuel cell," *Journal of The Electrochemical* Society, vol. 159, no. 5, pp.

B570-B577; 2012

[46] A. Malolepszy, M. Mazurkiewicz, L. Stobinski, B. Lesiak, L. Kövér, J. Tóth, B. Mierzwa, A. Borodzinski, F. Nitze, and T. Wågberg, "Deactivation resistant Pd-ZrO2 supported on multiwall carbon nanotubes catalyst for direct formic acid fuel cells," *International Journal of Hydrogen Energy*, vol. 40, no. 46, pp. 16724-16733; 2015

[47] R. K. Raman, N. A. Choudhury, and A. K. Shukla, "A high output voltage direct borohydride fuel cell," *Electrochemical and Solid-State Letters*, vol. 7, no. 12, pp. A488-A491; 2004

[48] D. Joubert; "Density Functionals: Theory and Application", *Lecture Notes in Physics*, Springer-Verlog, Berlin; 1998

[49] M. Mavrikakis, B. Hammer, & J.K. Norskov; "Effect of Strain on the Reactivity of Metal Surfaces", *Phys. Rev. Lett.*, vol 81, pp. 21819; 1998

[50] Y. Xu & M. Mavrikakis; "Adsorption and dissociation of O_2 on Cu(111) : thermochemistry, reaction barrier and the effect of strain"; *Surface Science*, vol. 494, Issue 2, pp. 131-144; 2001

[51] J. Greeley & M. Mavrikakis; "Methanol Decompostions on Cu(111): A DFT Study"; *Journal of Catalysis*; vol. 208, Issue 2, pp. 291-300; 2002

[52] T. Watanabe, M. Ehara, K. Kuramoto, & H. Nakatsuji; "Possible reaction pathway in methanol dehydrogenation on Pt and Ag surfaces/clusters starting from O-H scission: Dipped adcluster model study"; *Surface* Science; Vol. 603, Issue 4, pp. 641-646; 2009

[53] D. Cao, G.-Q. Lu, A. Wieckowski, S. A. Wasileski, M. Neurock; "Mechanisms of Methanol Decomposition on Platinum: A Combined Experimental and ab Initio Approach"; *Journal of Physical Chemistry*; vol 103, pp. 11622-11633; 2005

[54] I. P. Zaragoza, R. Salcedo, & J. Vergara; "DFT: a dynamic study of the interaction of ethanol and methanol with platinum"; *Journal of Molecular Modeling*; vol. 15, pp. 447; 2009

[55] M. J. Janik, C. D. Taylor, & M. Neurock; "First Principles Analysis of the Electrocatalytic Oxidation of Methanol and Carbon Monoxide"; *Topics in Catalysis*, vol. 46, Issue 3-4, pp. 306-319; 2007

[56] F. Vigier, S. Rousseau, C. Coutanceau, J.-M. Leger, & C. Lamy; "Electrocatalysis for the direct alcohol fuel cell", *Topics in Catalysis*; vol. 40; Issue 1-4; pp. 111-121; 2006

[57] F. Vigier, C. Coutanceau, F. Hahn, E.M. Belgsir, & C. Lamy; "On the mechanism of ethanol electro-oxidation on Pt and PtSn catalysts: electrochemical and in situ IR reflectance spectroscopy studies"; *Journal of Electroanalytical Chemistry*; vol. 563, Issue 1, pp. 81-89; 2004

[58] H.-F. Wang & Z.-P. Liu; “Comprehensive Mechanism and Structure-Sensitivity of Ethanol Oxidation on Platinum: New Transition-State Searching Method for Resolving the complex Reaction Network”; *Journal of the American Chemical Society*; vol. 33, pp. 10996-11004; 2008

[59] A. Kowal, M. Li, M. Shao, K. Sasaki, M.B. Vukmirovic, J. Zhang, N. S. Marinkovic, P. Liu, A. I. Frenkel, & R. R. Adzic; “Ternary Pt/Rh/SnO_2 electrocatalysts for oxidizing ethanol to CO_2”; *Nature Materials*; vol 8, pp. 325-330; 2009

[60] B. Delley; “An all-electron numerical method for solving the local density functional for polyatomic molecules”, *The Journal of Chemical Physics*; vol 92; pp. 508; 1990

[61] E. J. Cairns; “Hydrocarbon Fuel Cells with Fluoride Electrolytes”, *The Electrochemical Society*; vol 113; Issue 11; pp. 1200-1204; 1966

[62] N. M. Galea, D. Knapp, & T. Ziegler; “Density functional theory studies of methane dissociation on anode catalysts in solid-oxide fuel cells: Suggestions for coke reduction”; *Journal of Catalysis*; vol 247; Issue 1; pp. 20-33; 2007

[63] G. Psofogiannakis, A. St-Amant, & M. Ternan; “Methane Oxidation Mechanism on Pt(111): A Cluster Model DFT Study”; *Journal of Physical Chemistry*; vol 110, pp. 24593-24605; 2006

[64] V. S. Bagotzky, Y. B. Vassiliev, & O.A. Khazova; “Generalized scheme of chemisorption, electrooxidation and electroreduction of simple organic compounds on platinum group metals”; *Journal of Electroanalytical Chemistry and Interfacial Electrochemistry*; vol 81, Issue 2, pp. 229-238; 1977

[65] M. J. Janik & M. Neurock; “A first principles analysis of the electro-oxidation of CO over Pt(111)”; *Electrochimica Acta*; vol 52; Issue 18; pp. 5517-5528; 2007

[66] P. Ferrin, A. U. Nilekar, J. Greeley, M. Mavrikakis, & J. Rossmeisl; “Reactivity descriptors for direct methanol fuel cell anode catalysts”; *Surface Science*; vol 602; issue 21, pp. 3424-3431; 2008

[67] J. Mukherjee & S. Linic; “First-Principles Investigations of Electrochemical Oxidation of Hydrogen at Solid Oxide Fuel Cell Operating Conditions”; *Journal of the Electrochemical Society*; vol 154; issue 9; pp. B919-B924; 2007

[68] J. H. Pacheco, A. Bravo, O. Novara; “An ab initio study of platinum hydrogen interaction”; *Revista mexicana de fisica*; vol 52; Issue 5; pp. 394; 2006

[69] P. Ferrin, A. U. Nilekar, J. Greeley, M. Mavrikakis, & J. Rossmeisl; “Reactivity descriptors for direct methanol fuel cell anode catalysts”; *Surface Science*; vol 602; issue 21; pp. 3424-3431; 2008

[70] J. Kua & W. A. Goddard; "Oxidation on 2nd and 3rd Row Group VIII Transition Metals (Pt, Ir, Os, Pd, Rh, and Ru): Application to Direct Methanol Fuel Cells"; *Journal of the American Chemical Society*; vol 121; pp. 10928-10941; 1999

[71] E. Christoffersen, P. Liu, A. Ruban, H. L. Skriver, & J. K. Nørskov; "Anode Materials for Low-Temperature Fuel Cells: A Density Functional Theory Study"; *Journal of Catalysis*; vol 199; issue 1, pp. 123-131; 2001

[72] J. Rossmeisl & W. G. Bessler; "Trends in catalytic activity for SOFC anode materials"; *Solid State Ionics*; vol 178; issues 31-32; pp. 1694-1700; 2008

[73] T. G. Kelly; A. L. Stottlemyer; H. Ren; & J. G. Chen; "Comparison of O-H, C-H, and C-O Bond Scission Sequence of Methanol on Tungsten Carbide Surfaces Modified by Ni, Rh, and Au", *The Journal of Physical Chemistry*; vol 115; pp. 6644-6650; 2011

[74] D. V. Esposito & J. G. Chen; "Monolayer platinum supported on tungsten carbides as low-cost electrocatalysts: opportunities and limitations"; *Energy Environ. Sci.*; vol 4; pp. 3900-3912; 2011

[75] E. Nikolla, J. Schwank, & S. Linic; "Promotion of the long-term stability of reforming Ni Catalysts by surface alloying"; *Journal of Catalysis*; vol 250, issue 1; pp. 85-93; 2007

[76] M. B. Vukmirovic, J. Zhang, K. Sasaki, A. U. Nilekar, F. Uribe, M. Mavrikakis, & R.R. Adzic; "Platinum monolayer electrocatalysts for oxygen reduction"; *Electrochimica Acta*; vol 52; issue 6, pp. 2257-2263; 2007

[77] J. K. Nørskov, J. Rossmeisl, A. Logadottir, L. Lindqvist, J. R. Kitchin, T. Bligaard, & H. Jonsson; "Origin of the Overpotential for Oxygen Reduction at a Fuel-Cell Cathode"; *The Journal of Physical Chemistry*; vol 108, pp. 178886-17892; 2004

CHAPTER 3

THE USE OF DENSITY FUNCTIONAL THEORY TO OBSERVE ADSORPTION STATES

3.1. Introduction

A fuel cell is an electrochemical cell that converts the chemical energy from a fuel into electrical energy through an electrochemical reaction of the fuel with an oxidizing agent (usually oxygen from air) [1]. Fuel cells differ from batteries in that they require a continuous source of fuel and oxygen to sustain the electrochemical reaction [2]. Fuel cells can produce electrical energy continuously for as long as fuel and oxygen are supplied.

Fuel cells all consist of an anode, a cathode, and an electrolyte that allows for positively charged hydrogen ions (protons) to move from the anode to the cathode. At the same time, electrons are drawn from the anode to the cathode through an external circuit, producing direct current electricity. At the cathode, the hydrogen, electrons, and oxygen combine to form water as a product [3]. The different types of commercial fuel cells include proton exchange membrane (PEM), alkaline fuel cells, phosphoric acid fuel cells, molten carbonate fuel cells, and solid oxide fuel cells [4]. The main difference between these types of fuel cells is the electrolyte layer that is used. The PEM fuel cell type is the one used most frequently, and the work of this chapter is based on the use of a PEM fuel cell.

In PEM fuel cells hydrogen gas is the primary fuel source at the anode and oxygen from air is the oxidizing agent at the cathode. However, the majority of hydrogen gas is produced through the steam reforming of methane gas to form carbon dioxide and hydrogen gas [5]. In this

study, the hydrocarbons will be used in the fuel cell directly. This eliminates the step of steam reforming and a substantial capital investment.

There are many hydrocarbon fuels available for use in industry. One is ethane. It is widely used as a feedstock to create ethylene for plastic production. Ethylene is another fuel that is widely available due to the production of plastics. Previous fuel cell studies have shown that ethane reacts much slower than ethylene in fuel cells [6]. The purpose of this chapter is to compute the energies involved in the adsorption of hydrogen, ethane, and ethylene molecules on the catalyst surface.

Density Functional Theory (DFT) is a method that uses electron density to determine the ground state energy of a system of molecules [7]. Siesta uses the probability of an electron being found in a given location to determine the energy of the simulation system [8]. Since DFT can predict the ground state energies of simulation systems, the goal of this chapter is to use DFT to determine the energies involved in the adsorption of hydrogen, ethane, and ethylene molecules on the catalyst surface.

3.2. Computational Methodology

3.2.1. Density Functional Theory

Density Functional Theory (DFT) is a computational method that uses electron density to determine the ground state energy of a simulation system. It has gained popularity because the use of electron density limits the complexity of the calculation as compared to other approaches such as wave function methods. DFT is still limited by computational power [9]. More complex simulation systems take more time to converge to the lowest energy state due to the additional atoms included in the more complex systems. There are many software packages available that perform DFT calculations and the one selected for use in this work was SIESTA [8].

3.2.2. SIESTA

SIESTA (Spanish Initiative for the Electronic Simulation of Thousands of Atoms) is the software package that was selected for use to perform DFT calculations. It does so through an iterative method where it slowly moves atoms in different directions in order to minimize the ground state energy of the system. It was selected due to its ability to perform electronic structure calculations while providing control of the time, or cost, of each simulation by tuning several different factors: cut-off points at which the simulation can be said to have converged, step sizes, the maximum number of step sizes, and the number of k-points in the system. This permitted faster simulations for exploratory work and more fine-tuned simulations for calculations of final system simulation energies [8].

SIESTA represents each atomic species in the form of a pseudopotential. The purpose of the pseudopotential is to replace the core electrons with a potential [10]. Then electronic calculations are only performed on valence electrons. This is beneficial as it decreases the number of electronic calculations and thereby lowers the cost of the simulation while retaining the relativistic effects of the core electrons. There are different software applications available to create the pseudopotential files and the one selected for use in this work was ATOM.

3.2.3. ATOM

ATOM is the software package that was used to generate pseudopotential files for each atomic species for use by SIESTA to perform DFT calculations. It prepares the electronic configurations of atomic species [10]. The following are specified: number of core orbitals, number of valence orbitals, and for each valence orbital the following are specified: principal quantum number, angular momentum quantum number, and number of electrons located in each valence orbital. Several pseudopotential generation schemes are available in the software. The Troullier-Martins generation scheme was selected due to its simplicity compared to the other models.

ATOM also contains standard pseudopotential files and tests to compare the generated pseudopotential files to ones that are generally considered to be standard. This is done by

simulating molecules and atoms with the generated pseudopotential files, followed by comparison with the standard ones. Deviations between energy states and final geometries are noted. These tests are beneficial in ensuring that the generated pseudopotential files lead to accurate simulation results.

3.2.4. Methodology

Once a pseudopotential file has been created for each species, an input file for SIESTA can be created to specify how the simulation should proceed. The input file is used to specify which model should be used to perform the calculation, the locations of the individual atoms in the initial geometry of the system, and the constraints that determine when a simulation has reached convergence.

The convergence technique which SIESTA uses to perform DFT calculations needs to be specified in the input file. There are several convergence techniques available for use. Both the Broyden and the Conjugate Gradient convergence techniques were tested. The ground state energy of the system would oscillate without converging when using the Broyden convergence technique. Therefore, the Conjugate Gradient model was used for all simulations. The Conjugate Gradient convergence technique does not converge as quickly as the Broyden one. Compensation for this can be achieved by an increase in step size between iterations.

The cut-off point at which the simulation can be considered converged can also be specified and so can the size of the steps between each iteration. The larger the values of these specifications, the faster the simulation will converge. However, large values can also sacrifice the accuracy of the convergence. The more complicated geometries had difficulty converging, so the step sizes were constrained beyond the default value by a factor of 10 to limit oscillations and to permit the simulations to converge. This increased both the number of steps and the amount of time it took for the simulation system to converge, but it was necessary to reach a minimum energy.

The specification of the geometry of the unit cell and the location of individual atoms within the unit cell is also done in the input file. SIESTA uses repeating or periodic boundary conditions. If the unit cell is repeated in all three directions, a three dimensional solid is obtained. If the unit cell is repeated in only 2 directions a slab is formed. If the unit cell is not repeated at all a cluster is formed. Large amounts of vacuum are specified in the direction(s) that the unit cell should not be repeated. For example, specifying a large amount of vacuum in the z-direction will be interpreted as a slab calculation. SIESTA will then repeat the unit cell in the x- and y-directions. In the z-direction there will be a series of slabs each interspersed by a large amount of vacuum. Cluster calculations were used for individual molecules, while slab calculations were performed for any calculation involving a catalyst surface.

A bi-product of the unit cell size of and the slab size is the number of k-points in the simulation system. (k-points are sampling points in the first Brillouin zone.) The larger the unit cell, the more k-points there are in the system. The larger the slab size (the real-space cell) the smaller the reciprocal space and the fewer k-points needed. The number of k-points is a reflection of how fine the mesh is that SIESTA uses to perform its iterative calculations. Those simulations that have a larger number of k-points have a finer mesh. The number of k-points also affects the time required for each iteration in a ground state energy calculation. The more k-points in the system, the longer it takes to calculate each step. This increases the time it takes for the simulation to converge. However, having fewer k-points can lead to inaccurate results in the simulations. It is important to find a balance between time, or cost, and accuracy. 32 k-points were used in our simulations. With 32 k-points there was not much difference in ground state energy when the number of k-points was varied.

The positions of the individual atoms in the unit cell can be specified as fixed or relaxed. A fixed position is one that cannot move whereas a relaxed position is one that can be moved in order to minimize the energy of the system. Each coordinate of an atom needs to be specified as fixed or relaxed. This permits atoms to move in 3-dimensions, or on a plane, or along a line, or not at all. Fixing atom positions can be useful in controlling the cost of a simulation. Each fixed atom means there is one less atom for which movement must be calculated. However, it does not

reflect reality. In particular, the surface atoms of a catalyst are free to move in any direction. Similar to k-points, a balance needs to be found between cost and accuracy.

When optimizing molecules or atoms, the atoms are specified as relaxed in all directions to yield the optimal geometry. Simulating molecules or atoms is fast as the systems do not contain many atoms. This allows for the calculation to converge quickly even when all the atoms are relaxed in all directions. These calculations are useful as they give the ground state energy of the molecule or atom in the gas form.

After the molecules were optimized, the nickel catalyst slab was optimized. Due to the amount of nickel atoms in the slab, it was decided not to relax the nickel atoms and keep them at the same positions they have the crystalline structure of bulk nickel. This is not an accurate representation of surface nickel atoms since they do not retain the bulk crystalline structure. However, this decision was made to simplify future adsorption runs and reduce the cost of each simulation. Allowing the nickel atoms to relax drastically increases the time the simulation takes to converge. Also, many more initial orientations of the substrate molecules on the surface of the catalyst are possible. The simulations of the nickel slab by itself gave the ground state energy of the catalyst slab.

In adsorption runs, the atoms in the molecules are placed over the nickel slab at a fixed distance. The distance is fixed with respect to one atom and the coordinates of the other atoms are relaxed. As adsorption is energetically favourable, the molecule would be brought closer to the catalyst by density functional theory as it is brought to a more energetically stable location. Fixing the location allows for the difference in energy to be observed. Gradually allowing the molecule to approach the catalyst and noting the difference in system energy allows for adsorption to be studied.

3.3. Results and Discussion

3.3.1. Adsorption Curve

Adsorption occurs because the energy of a system is lower when a molecule is bound to a surface than when the molecule is separate from the surface. This process releases energy and this release of energy allows for adsorption to occur. As Density Functional Theory calculates the entire energy of a system, it is possible to compare differences in the overall system energy at different system geometries. Comparing the energy of the system when a molecule is placed over a surface (the adsorbed phase) to the energy of the system when a molecule is at an infinite distance from the surface (the gas phase) shows how much energy is released when the molecule adsorbs on the surface. The purpose of making the adsorption computations is to identify the geometries having the minimum energies.

To begin, a single molecule (e.g., ethylene) was simulated using Density Functional Theory. Independently, a Ni-catalyst slab was simulated using Density Functional Theory. Adding the energy of the molecule and the energy of the slab provides the combined energy of the molecule in the gas phase and the energy of the isolated Ni slab. A simulation was also made with the molecule placed on the surface of the Ni slab. The combined energy of the gas phase molecule and the isolated Ni slab was subtracted from the energy of the molecule and Ni slab when the molecule was adsorbed on the slab. The resulting decrease in energy (or release of energy) of the system is the heat of adsorption.

Computations were performed with the molecule located at various distances from the catalyst surface. As the molecule moves progressively closer to the surface, the energy of the system decreases, reaches a minimum, and increases again. This behaviour is seen in Figure 3.1 The geometry with minimum energy is the geometry at which the molecule is adsorbed on the catalyst surface.

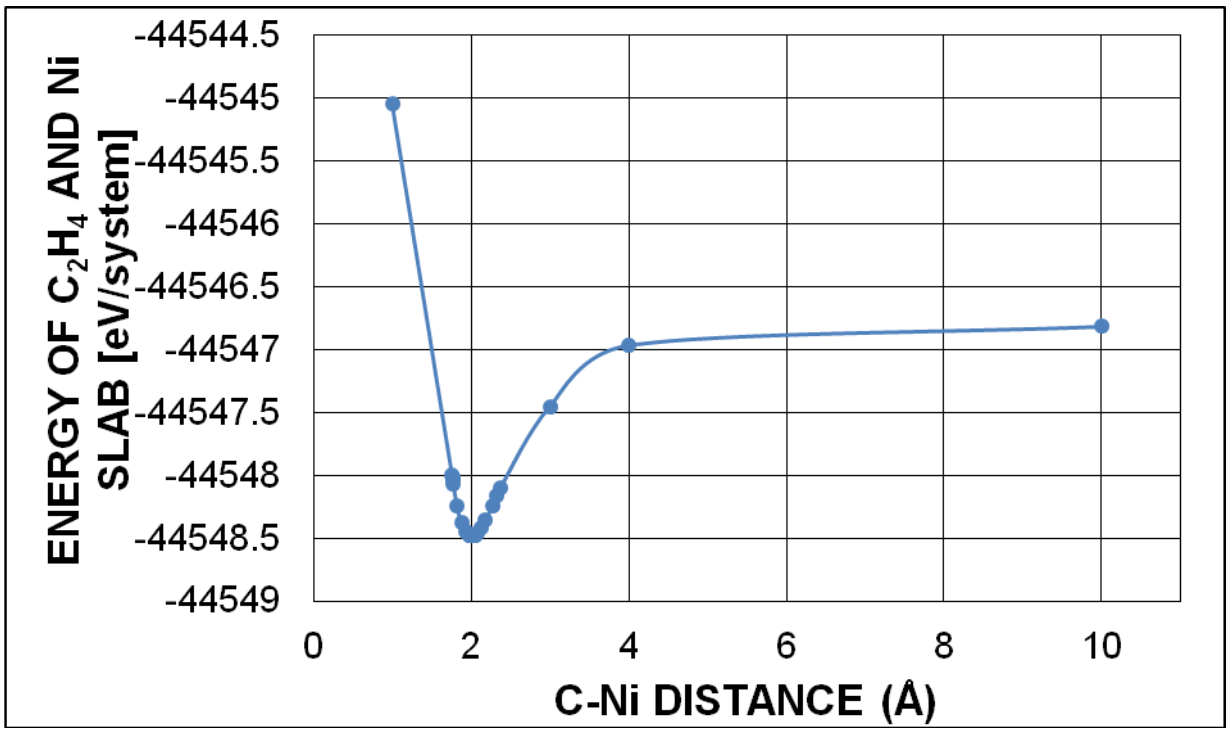

Figure 3.1: System Energy (eV) vs Carbon-Nickel Distance (Å) in the Adsorption of Ethylene on Nickel

The difference between the combination of isolated molecule plus isolated Ni-slab and the energy of the adsorbed state (molecule adsorbed on Ni-slab) is the heat of adsorption, for the molecule on that particular catalyst surface. To better visualize the energy differences, subtracting the energy of the molecule in the gas phase and the energy of the catalyst slab from the system energy with the molecule adsorbed onto the catalyst produces the heat of adsorption versus the carbon-nickel distance as seen in Figure 3.2.

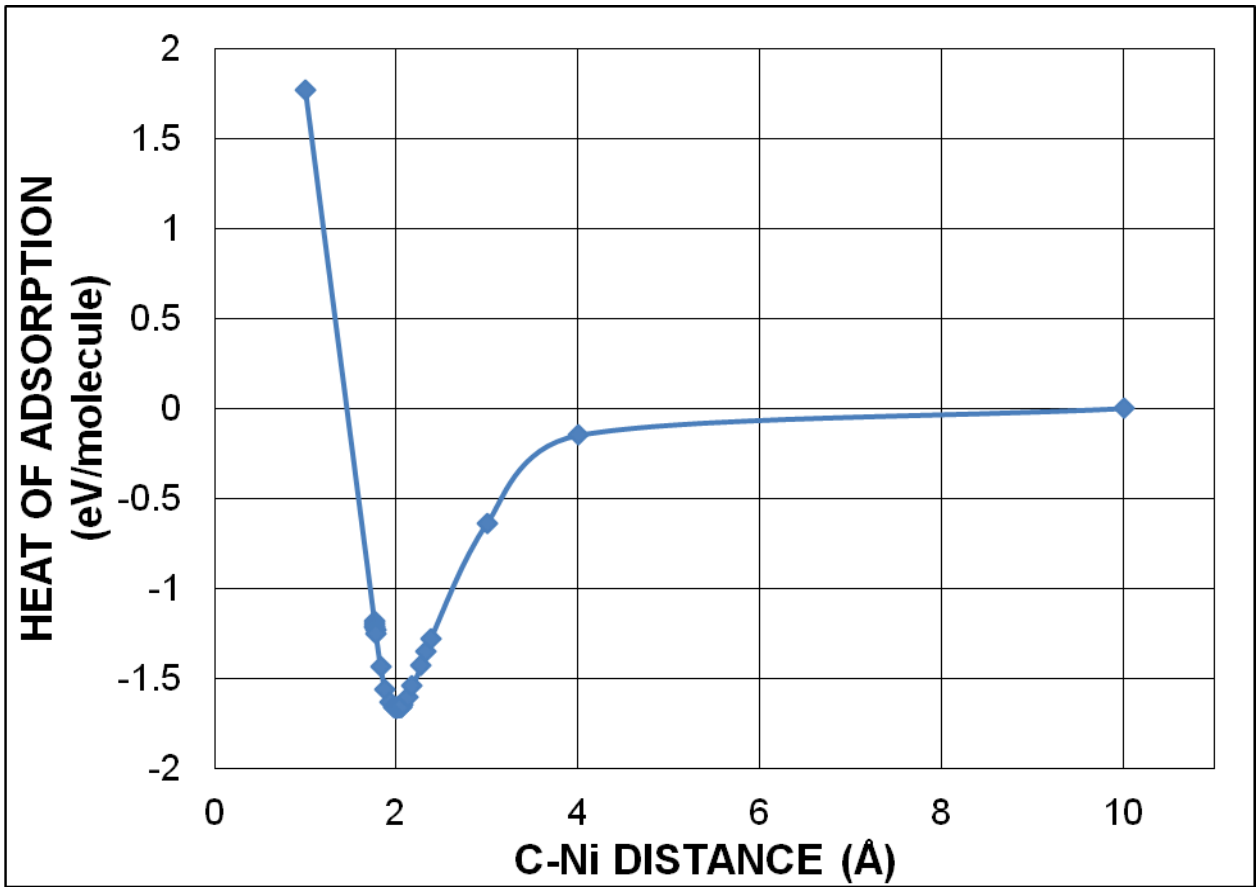

Figure 3.2: Heat of Adsorption (eV/molecule) vs Carbon-Nickel Distance (Å) in the Adsorption of Ethylene on Nickel

3.3.2. Geometry Study

3.3.2.1 Effect of Initial Orientation

Density Functional Theory minimizes the overall energy of the system. It achieves this by changing the location of atoms gradually until there is no further decrease in the energy of the system. However, it is possible that the final energy and geometry of the system is a local minimum and not the actual lowest overall energy. The only way to compensate for this is to try different initial geometries to determine which leads to the absolute minimum of the system. Simulating the adsorption of ethylene on a nickel catalyst using different initial orientations of

the ethylene molecule was done to investigate the effect of initial geometry on the heat of adsorption

Three different initial geometries were chosen based on the location of the ethylene carbon-carbon double bond in respect to the surface of the nickel catalyst. These geometries shown in Figure 3.3 below. In Geometry 1, the double bond is located over a valley between two adjacent nickel atoms. The two carbons are arranged in such a way that the bond between them is perpendicular to the bond between the two nickel atoms. In Geometry 2, the double bond is also located over a valley between two adjacent nickel atoms. However, the two carbon atoms are arranged in such a way that the bond between them runs parallel to the bond between the two nickel atoms. In Geometry 3, the double bond is centered on top of a nickel atom with the hydrogen atoms as close as possible to the valley between four nickel atoms. With this geometry, the location of the two carbon atoms plays no role as they are both bonding to the same nickel atom. If the molecule is rotated 90^o, 180^o, or 270^o the hydrogen atoms will still be as close as possible to the valley between the four nickel atoms.

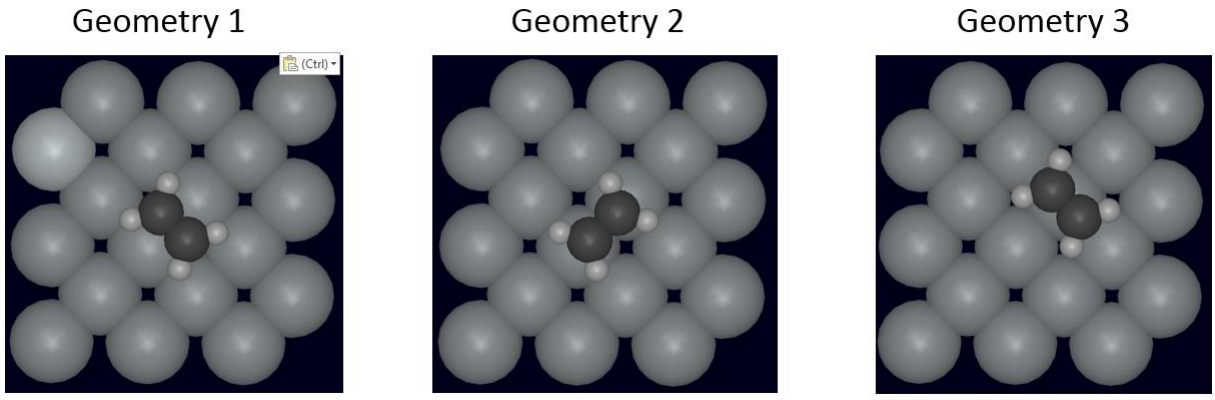

Figure 3.3: Varying Geometries of Ethylene over Nickel

In comparing the heat of adsorptions that were achieved from these three different geometries, it was discovered that Geometry 2 was the geometry that had the largest heat of adsorption. All subsequent adsorption runs were performed with this initial geometry. The same geometry was applied to ethane adsorption calculations due to similarities between the structures of ethane and ethylene.

3.3.2.2 Effect of Slab Size

The size of the nickel catalyst slab is also a representation of the catalyst coverage. The smaller the slab size (i.e., the smaller the number of surface nickel atoms), the higher the catalyst coverage. Any specific slab size may not necessarily reflect the amount of ethylene that adsorbs onto the catalyst surface in an actual fuel cell. Small slab sizes lead to higher probabilities of ethylene atoms interacting with each other and not just the nickel catalyst slab. The object of this work was to understand the interaction of a single molecule with a Ni slab. A slab size large enough to avoid interactions between adsorbed molecules was desired. For these reasons, five runs with different slab sizes were performed to observe the effect coverage can have on the heat of adsorption. Some of these slab sizes are shown in Figure 3.4.

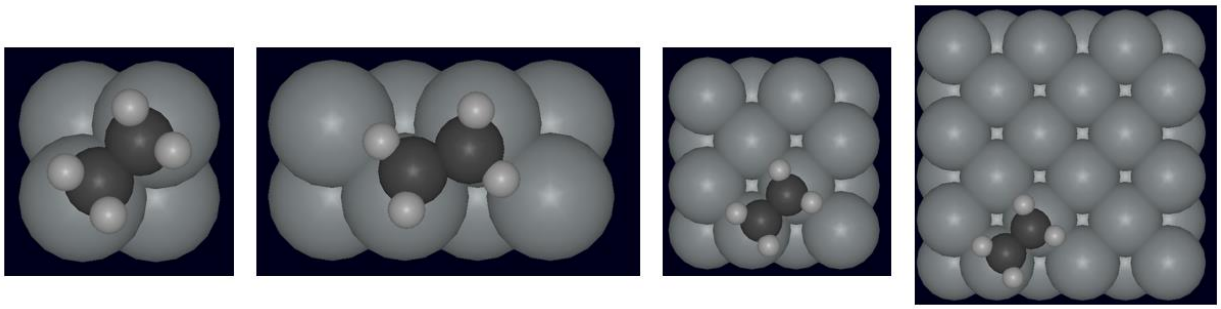

Figure 3.4: Varying Sizes of Ethylene Adsorbed on Nickel Slabs

The five different nickel catalyst slab sizes consisted of 2, 4, 8, 18, and 32 surface nickel atoms. However, for nickel catalyst slab sizes with 2 or 4 nickel atoms the heat of adsorption changed. In addition, the geometry of the adsorbed ethylene atom also changed. This is due to crowding and interactions between neighbouring ethylene molecules. This is most noticeable in the nickel slab with 4 surface nickel atoms. There is a visible twisting in the orientation of the ethylene molecule. Slab sizes with 8 or more surface nickel atoms all had the same heat of adsorption, as seen in Figure 3.5. This is an important finding as simulations of hydrocarbon adsorption by Density Functional Theory that are reported in the literature [11] tend to use high coverages of the catalyst surface. Studies with high surface coverages where the adsorbed molecules interact with one another are important. Nevertheless, the base case for a comparison should always be a simulation where the single molecule-slab interactions are not influenced by

interactions between adsorbed molecules. With 2 surface Ni atoms the calculated heat of adsorption is endothermic. In their review, Hayward and Trapnell [12] reported that no case of endothermic adsorption is definitely known.

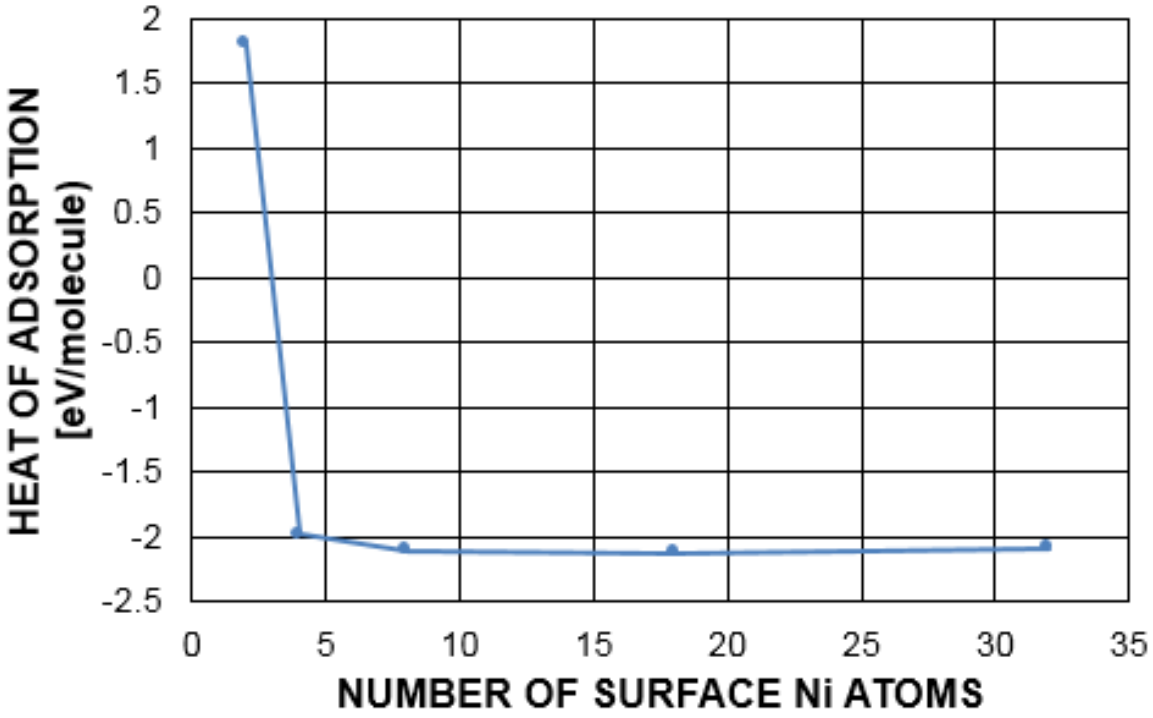

Figure 3.5: Heat of Adsorption (eV) vs Number of Surface Nickel Atoms for Ethylene Adsorption

3.3.2.3 Effect of Nickel Slab Thickness

Several studies in the literature have placed great emphasis on the thickness of the catalyst slab in literature, in some cases reaching as deep as seven layers [13]. Simulations using multiple layers increases the computation time, or cost, of the simulation. In order to minimize the cost of each simulation, a study was done with nickel catalyst slabs at four different thicknesses to observe the effect of different layers on the heat of adsorption.

Adsorption runs were performed on 1, 2, 3, and 4 layer nickel catalyst slabs with the same orientation of ethylene on the surface. Two of these adsorption geometries are shown in Figure 3.6.

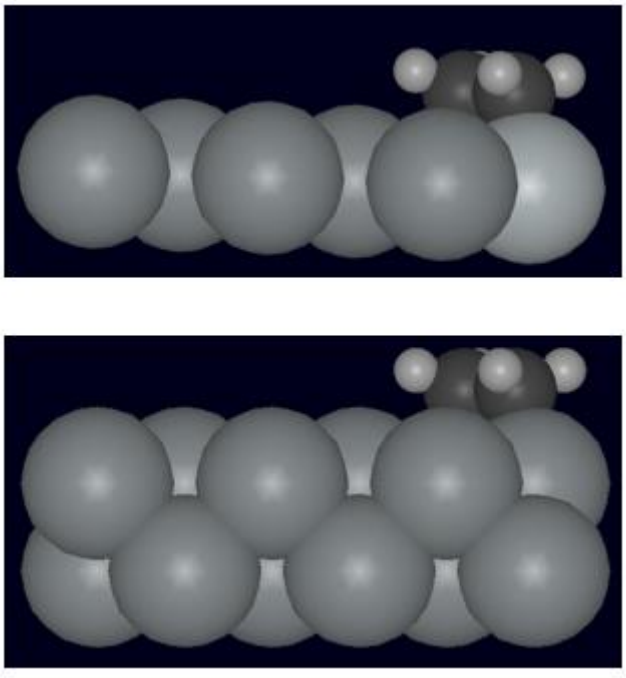

Figure 3.6: Ethylene Adsorbed onto a 1- and 2-layer Thick Nickel Catalysts

The largest energy was obtained using a nickel catalyst with only 1 layer. The most likely reason for this is that a vacuum exists on both sides of the nickel layer, allowing for more charges to be shared from this nickel atom. Increasing the nickel thickness to 2 or more layers increases the cost of the simulation and decreases the heat of adsorption. The heats of adsorption obtained for each slab thickness are shown in Figure 3.7.

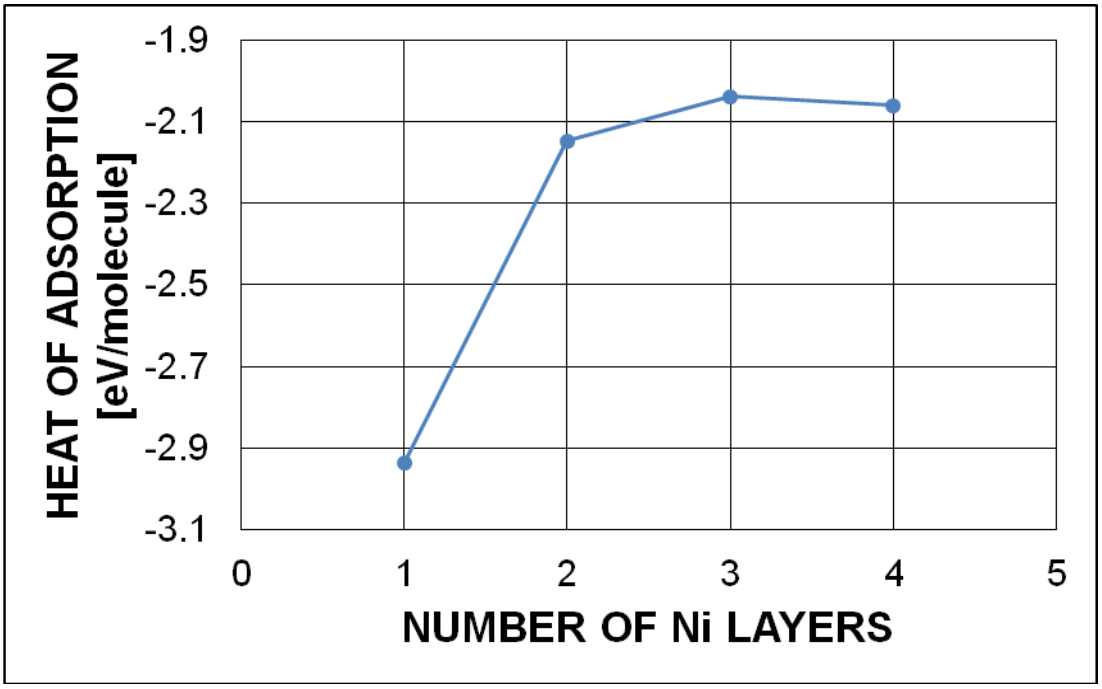

Figure 3.7: Heat of Adsorption (eV/molecule) vs Number of Ni Layers

The geometry of the adsorbed ethylene molecule as a function of the number of layers in the nickel catalyst slab was examined. This was done by calculating the carbon-carbon bond length after the simulation was finished. It was noted that there was no change in the final carbon-carbon bond length of the ethylene molecule when the number of layers of nickel catalyst changed.

3.3.3. Mulliken Population Analysis

3.3.3.1 Ethylene Adsorption

A Mulliken Population Analysis was performed on both ethylene and a nickel catalyst slab in order to determine the charged distribution between the atoms. The number of valence electrons shared by an atomic species is related to the distribution of charges after adsorption has occurred. For instance, a hydrogen atom has one valence electron, giving it a charge of 1. Carbon has 4 valence electrons and a charge of 4. A nickel atom has 10 valence electrons, giving it a charge of 10. Any changes from these charge numbers indicates movement of charges from one atom to another. The charges on the isolated Ni-slab and the gas phase ethylene molecule are shown in Figure 3.8 and Figure 3.9, respectively. However, the gas phase ethylene molecule in

Figure 3.9 had some of the charges from the carbon atoms (4 to 3.483) move to the hydrogen atoms (1 to 1.259).

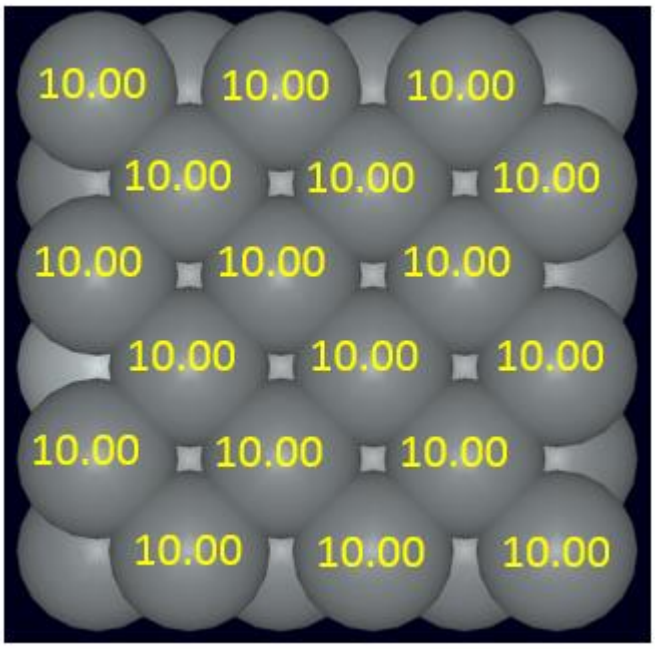

Figure 3.8: Charge Distribution of Surface Nickel Atoms

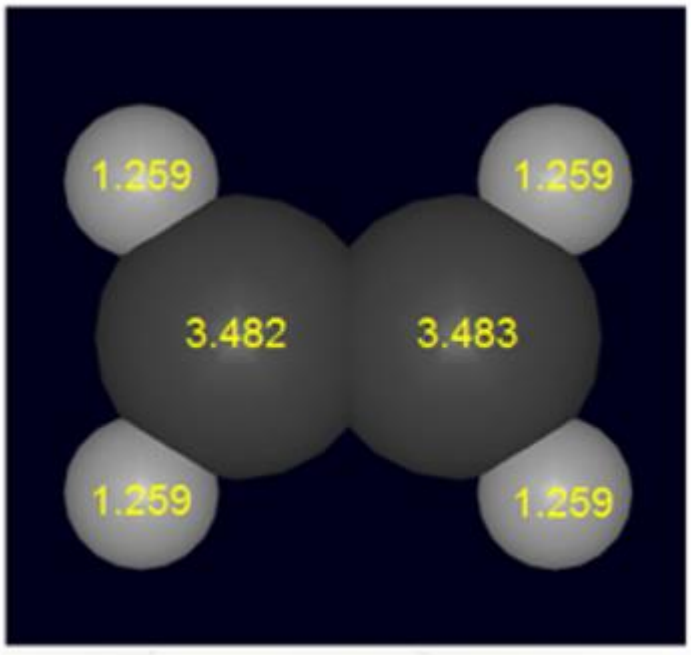

Figure 3.9: Charge Distribution in a Molecule of Ethylene

A change in charge is calculated by comparing the charge on an atom before adsorption with the charge on the same atom after adsorption. Any deviation from the charge distribution before adsorption indicates a movement of charges. After adsorption the nickel catalyst slab had donated some of its initial charge to the ethylene molecule. Although the hydrogen atoms obtained some additional charge, the majority of the charge lost by the nickel catalyst slab was donated to the carbon atoms of the ethylene molecule. This is seen in Figure 3.10 In the figure, all charge differences are multiplied by a factor of 1000. For example, the charge difference on the carbon atom of 92 in Figure 3.10 would correspond to a charge difference of 0.092 in Figure 3.9 .

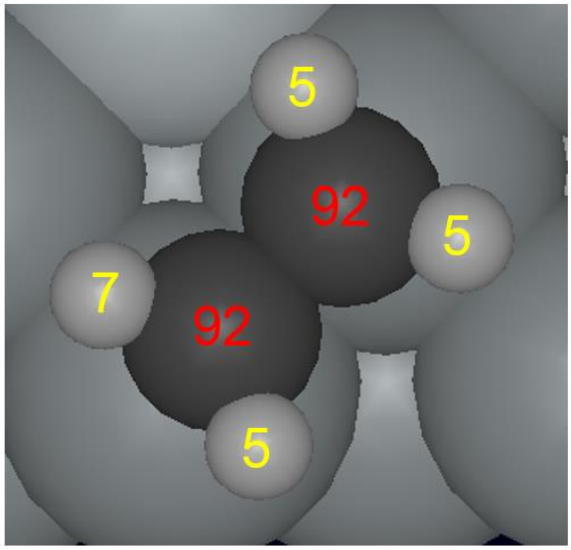

Figure 3.10: Charge Gained by the Atoms of an Ethylene Molecule Adsorbed onto Nickel

The surface coverage of the catalyst slab appears to have an effect on the way charges are shared. Six surface atoms of the nickel catalyst slab provided almost all of the charges to the ethylene molecule. This 6-atom site is shown in Figure 3.11. Due to the periodic (repeating) boundary conditions, the nickel atom at the top of the figure with a shared charge (-53) is identical to the sixth nickel atom that would be part of the same adsorption site as the other five nickel atoms at the bottom left of the figure. Again, all charge differences are multiplied by a factor of 1000.

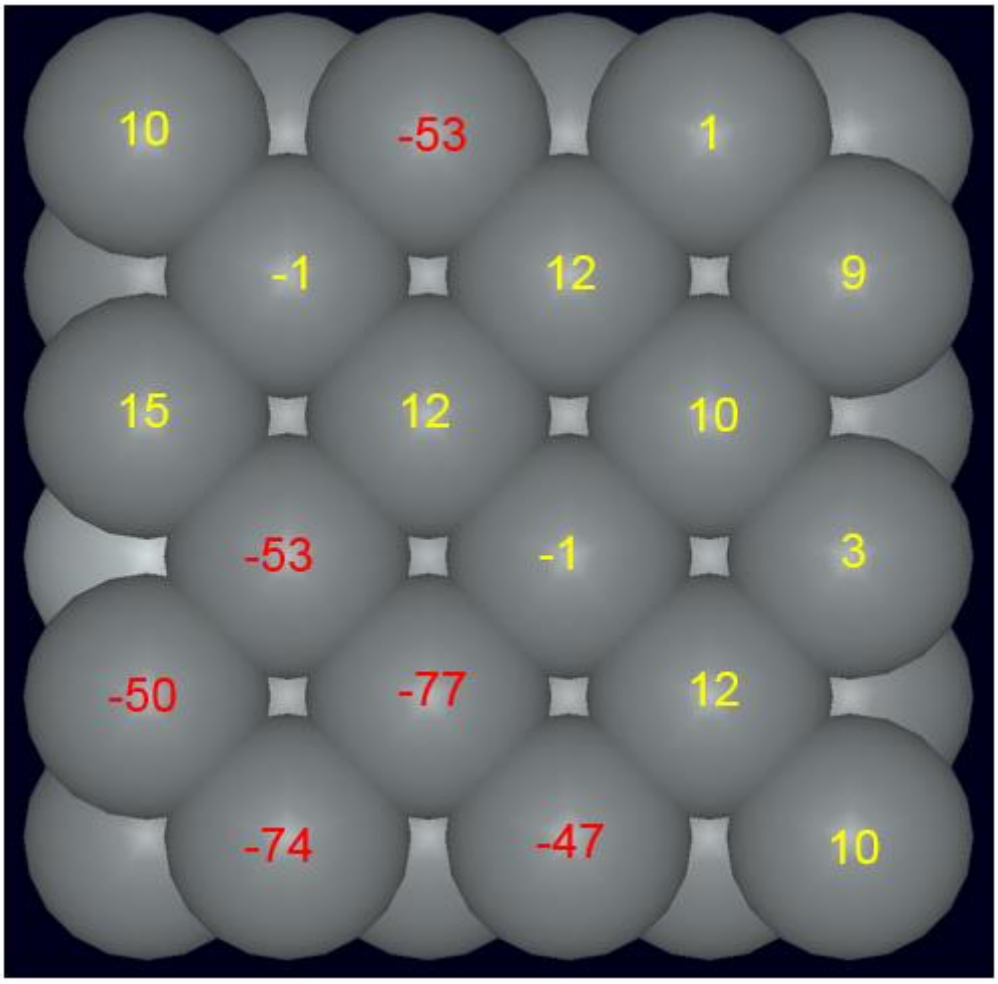

Figure 3.11: Charge Lost by Nickel Atoms to an Adsorbed Ethylene Molecule

This 6 nickel atom adsorption site for ethylene is an important observation. Several studies in the literature which used Density Functional Theory had fewer than 6 nickel atoms, for example [11]. Those studies represented higher surface coverages which means fewer surface nickel atoms to adsorb the ethylene molecule. The data in Figures 3.10 and 3.11 indicate that an ethylene molecule can have an adsorption site that consists of six nickel atoms. The 6-atom adsorption site was observed when there were 8, 18, and 32 surface nickel atoms. The amount of charge shared by the atoms was different in the 8 surface atom slab than in the larger catalyst slab sizes of 18 and 32 surface nickel atoms. The amount of charge shared between the six nickel atoms and the ethylene molecule was the same for each atom at the two largest catalyst slab sizes of 18 and 32 surface nickel atoms.

3.3.3.2 Ethane Adsorption

A Mulliken Population Analysis was performed on ethane in the gas phase and adsorbed ethane to determine charge distribution. This combined with the knowledge of the charge distribution in the metal catalyst slab allowed for the flows of charge to be observed. It appears that charge flows from the nickel catalyst into the two carbon atoms of the adsorbed ethane molecule with the carbon atom which has two hydrogen atoms facing the catalyst slab taking slightly more charge than the carbon atom which has one hydrogen atom facing the catalyst slab. Charge also flows from the catalyst slab to the three hydrogen atoms facing the nickel catalyst slab. As the ethane molecule is not symmetrical, neither is the charge flow to the hydrogen atoms. One carbon atom has two hydrogen atoms facing the nickel catalyst slab and one carbon atom has one hydrogen atom facing the nickel catalyst slab. The latter hydrogen atom has the most charge that flows to it of all atoms in the ethane molecule. Roughly 60 % of the amount of charge that flows to this hydrogen atom flows to each of the other two hydrogen atoms facing the nickel catalyst slab, which happens to be a similar amount of charge that flows to the carbon atoms. Little charge flows to the three hydrogen atoms facing away from the nickel catalyst slab in comparison to the other atoms in adsorbed ethane. This is seen in Figure 3.12. In the figure, all charge differences are multiplied by a factor of 1000.

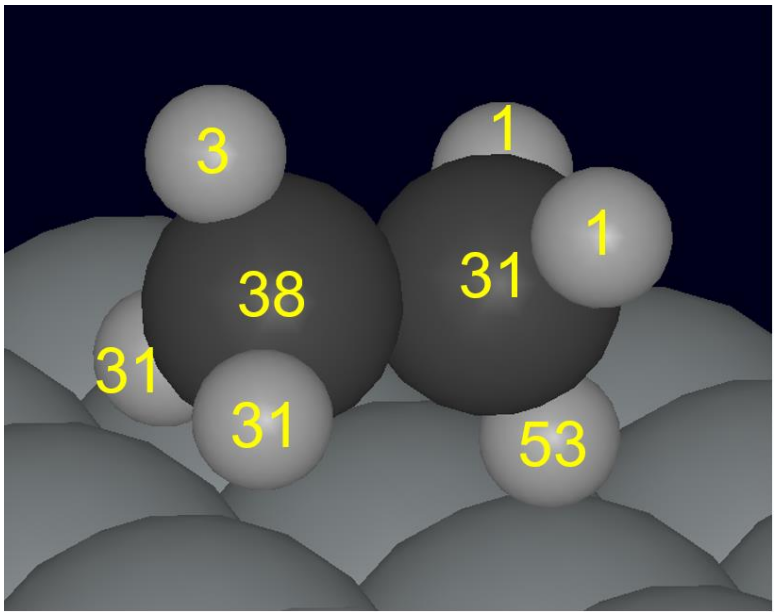

Figure 3.12: Charge Gained by the Atoms of an Ethane Molecule Adsorbed onto Nickel

The charge that flows to the adsorbed ethane molecule appears to originate from four (4) nickel atoms: the two atoms directly under the ethane molecule and the two adjacent nickel atoms next to the nickel atom which is under the carbon atom with two hydrogen atoms facing it in the adsorbed phase. The majority of the charge from comes from the two nickel atoms located directly under the adsorbed ethane molecule. Slightly more charge flows from the nickel atom which is under the carbon atom with two hydrogen atoms facing the nickel catalyst slab than the nickel atom which is under the carbon atom with one hydrogen atom facing the nickel catalyst slab. The charge differences for the two adjacent hydrogen atoms to the nickel atom from which the most charge flow originates (under the carbon atom with two hydrogen atoms facing the nickel catalyst slab) are an order of magnitude lower than the flow that originates from the two nickel atoms directly under the adsorbed ethane molecule. The 4-nickel atom adsorption site for ethane is an important observation for the same reasons outlined in Section 3.3.3.1 for ethylene adsorption. The 4-atom site is shown in Figure 3.13. Again, all charge differences are multiplied by a factor of 1000.

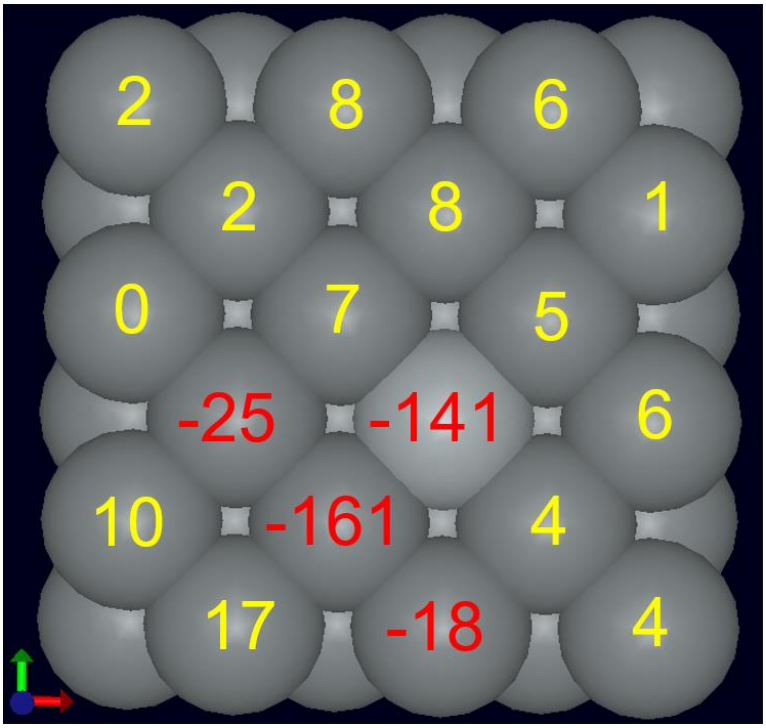

Figure 3.13: Charge Lost by Nickel Atoms to an Adsorbed Ethane Molecule

3.3.3.3 Hydrogen Adsorption

A Mulliken Population Analysis was performed on hydrogen in the gas phase and adsorbed hydrogen to determine the charged distribution between the atoms in each system. This combined with the knowledge of the charge distribution in the metal catalyst slab allowed for the flows of charge to be observed. It appears that charge flows from the nickel catalyst into the two hydrogen atoms of the adsorbed hydrogen molecule with roughly the same amount of charge flowing to each hydrogen atom. This is seen in Figure 3.14. In the figure, all charge differences are multiplied by a factor of 1000.

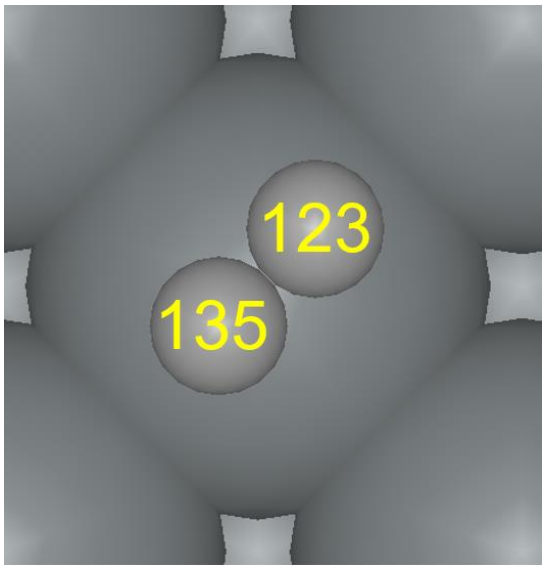

Figure 3.14: Charge Gained by the Atoms of a Hydrogen Molecule Adsorbed onto Nickel

The surface coverage of the catalyst slab appears to have an effect on the way charges are shared. Five (5) surface atoms of the nickel catalyst slab provided almost all of the charges to the hydrogen molecule, with the majority of the flow originating from the nickel atom directly underneath the adsorbed hydrogen atom. The flow of charge from each of the 4 nickel atoms adjacent to the nickel atom located directly underneath the adsorbed hydrogen molecule is an order of magnitude lower than the amount of flow that originates from the nickel atom directly under the adsorbed hydrogen molecule. Of the 4 adjacent nickel atoms, two are in line with they

adsorbed hydrogen molecule (this makes them closer to the hydrogen atoms) and two are not (further from the hydrogen atoms). Twice the amount of charge flow comes from the nickel atoms in line with (closest to) the adsorbed hydrogen molecule than the amount of flow from the two nickel atoms further from the adsorbed hydrogen molecule. This 5-atom site is shown in Figure 3.15. Again, all charge differences are multiplied by a factor of 1000.

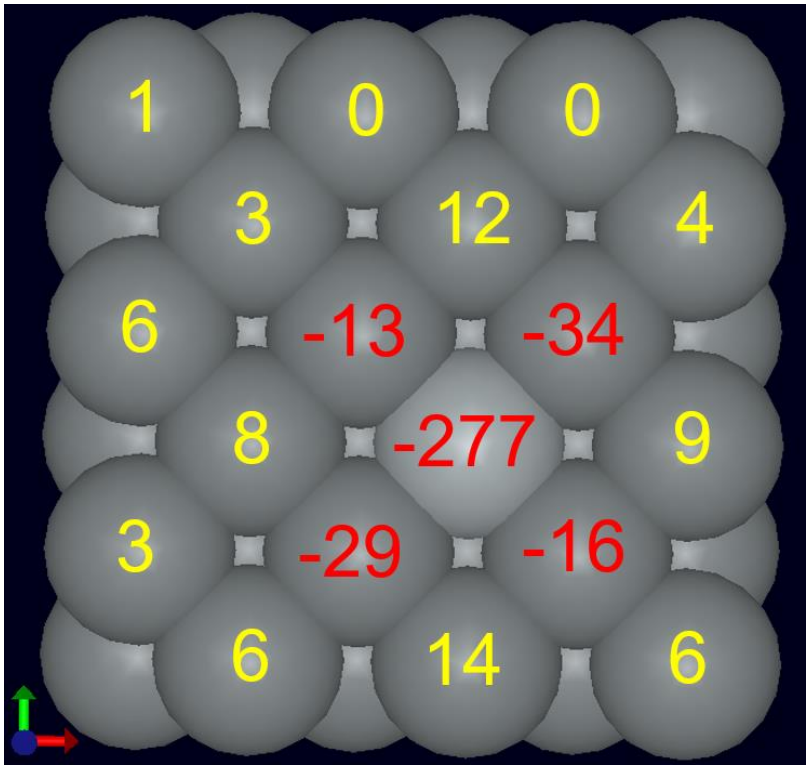

Figure 3.15: Charge Lost by Nickel Atoms to an Adsorbed Hydrogen Molecule

3.3.4. Adsorption Results

Four different species were simulated to determine their heats of adsorption. These were atomic hydrogen, hydrogen gas, ethylene, and ethane. The heats of adsorption were found to be -68.70 kJ/mol for ethane, -96.48 kJ/mol for hydrogen gas, -213.7 kJ/mol for ethylene, and -394.0 kJ/mol for atomic hydrogen. These heats of adsorption are represented in Figure 3.16 below.

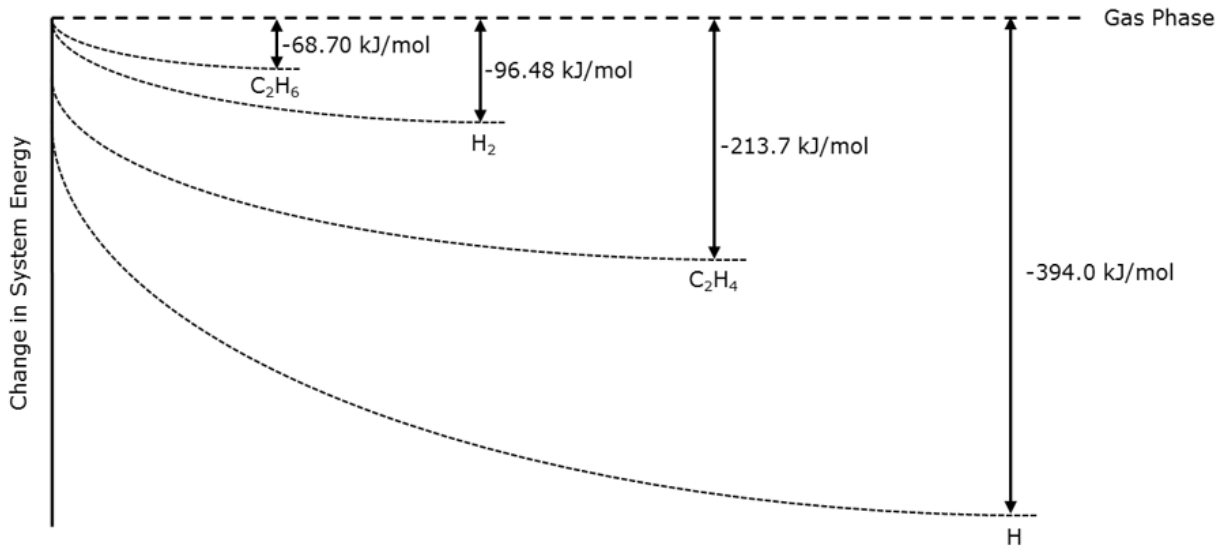

Figure 3.16: Heats of Adsorption of Different Species

These heats of adsorption indicate that atomic hydrogen is the most strongly bound to the nickel catalyst surface. Ethylene gas is next, followed by hydrogen gas and ethane gas. The difference between the heats of adsorption of ethylene and ethane may help explain why ethylene tends to react more quickly in a fuel cell as compared to ethane.

3.4 Conclusions

The major finding was the fact that the adsorption site for an ethylene molecule consisted of 6 nickel atoms. It was concluded the optimal initial orientation for the molecules is one where the bond between the two carbon atoms is located over a valley between two nickel atoms. The two carbons were placed in parallel to the two nickel atoms that form the valley with one carbon atom on each nickel atom. This orientation yields the lowest system energy and, thus, releases the most energy when the molecule is adsorbed onto the nickel catalyst surface.

Catalyst slabs having two nickel layers produced results similar to thicker slabs. The differences in the heats of ethylene adsorption were less than 4 kJ/mol between 2-layer nickel catalyst slabs and 3- and 4-layer nickel catalyst slabs for the adsorption of ethylene. A difference of 4 kJ/mol when the ethylene heat of adsorption is 214 kJ/mol does not warrant the additional computation time. Therefore, 2-layer nickel catalyst slabs were used for simulations.

The effect of catalyst coverage on the heat of adsorption and the transfer of charges was also tested. A minimum of 8 nickel atoms on the slab surface were required in order to avoid effects of crowding on the heat of adsorption. However the ethylene adsorption site was composed of 6 nickel atoms. 18 surface nickel atoms in a slab rather than 8 surface nickel atoms diminished the possibility of interactions between ethylene molecules. For these reasons, it was concluded that a catalyst with a surface containing 18 nickel atoms would be used for simulations.

Atomic hydrogen is more strongly bound to nickel than ethylene, hydrogen gas, and ethane. Ethane is the least strongly bound out of the 4, while ethylene is second most strongly bound and hydrogen gas is third. The difference in the heat of adsorption between ethylene and ethane may help explain why ethylene reacts faster than ethane when used in a fuel cell.

3.5 References

[1] H. A. Liebhafsky and L. W. Niedrach, "Fuel cells," *Journal of The Franklin Institute*, vol. 269, no. 4, pp. 257-267, 1960.

[2] M. Winter and R. J. Brodd, "What are Batteries, Fuel Cells, and Supercapacitors?," *Chem. Rev.*, 104, pp. 4245-4270, 2004.

[3] R. O'Hayre et al., "Introduction", *Fuel Cell Fundamentals*, 3rd Edition, Wiley, USA, pp. 3-24, 2016

[4] M. L. Perry and T. F. Fuller, "A historical perspective of fuel cell technology in the 20th century," *Journal of The Electrochemical Society*, vol. 149, no. 7, pp. S59-S67, 2002.

[5] A.Demirbas, "Future hydrogen economy and policy", *Energy Sources, Part B: Economics, Planning, and Policy*, 12:2, pp. 172-181, 2017

[6] E.J. Cairn and D.I. Macdonald, *Electrochemical Technology 2*, 65-70, 1964

[7] W. Kohn, "Overview of Density Functional Theory", *Density Functional Theory*, edited by E. K. U. Gross and R. M. Dreizler, Springer Science+Business Media, USA, pp. 3-10, 1995

[8] E. Artacho et al., "SIESTA 2.0.2", Fundacion General University, Spain, 2008 (http://www.uam.es/siesta)

[9] N. Schuch and F. Verstraete, "Computational complexity of interacting electrons and fundamental limitations of density functional theory", *Nature Physics*, Vol. 5, pp. 732-735, 2009

[10] Garcia, A.; Atom User Manual, University of Pais Vasco, Spain, 2006 (http://nf.nci.org.au/facilities/software/Siesta/2.0/atom.pdf)

[11] C.J. Heard, S. Siahrostami, H. Grönbeck, "Structural and Energetic Trends of Ethylene Hydrogenation overTransition Metal Surfaces", *Journal of Physical Chemistry*, Series C, , vol. 120, pp. 995−1003, DOI: 10.1021/acs.jpcc.5b09735, 2016.

[12] D.O.Hayward, B.M.W. Trapnell, "Chemisorption", Butterworths, London, p. 1, 1964.

[13] A. A. Ramanathan, "A DFT Calculation of Nb and Ta (001) Surface Properties", *Journal of Modern Physics*, vol. 4, pp. 432-437, 2013

CHAPTER 4

THE USE OF DENSITY FUNCTIONAL THEORY TO EXPLORE TRANSITION STATES

4.1. Introduction

A fuel cell is an electrochemical cell that converts the chemical energy from a fuel into electrical energy through an electrochemical reaction of the fuel with an oxidizing agent (usually oxygen from air). [1] Fuel cells differ from batteries in that they require a continuous source of fuel and oxygen to sustain the electrochemical reaction. [2] Fuel cells can produce electrical energy continuously for as long as fuel and oxygen are supplied.

Fuel cells all consist of an anode, a cathode, and an electrolyte that allows for positively charged hydrogen ions (protons) to move from the anode to the cathode. At the same time, electrons are drawn from the anode to the cathode through an external circuit, producing a direct current electricity. At the cathode, the hydrogen, electrons, and oxygen combine to form water as a product [3]. The different types of commercial fuel cells include proton exchange membrane (PEM), alkaline fuel cells, phosphoric acid fuel cells, molten carbonate fuel cells, and solid oxide fuel cells [4]. The main difference between these types of fuel cells is the electrolyte layer that is used. The PEM fuel cell type is the one used most frequently, and the work of this chapter is based on the use of a PEM fuel cell.

In PEM fuel cells hydrogen gas is the primary fuel source at the anode and oxygen from air is the oxidizing agent at the cathode. However, the majority of hydrogen gas is produced through the steam reforming of methane gas to form carbon dioxide and hydrogen gas [5]. In this

study, the hydrocarbons will be used in the fuel cell directly. This eliminates the step of steam reforming and a substantial capital investment.

There are many hydrocarbon fuels available for use in industry. One is ethane. It is widely used as a feedstock to create ethylene for plastic production. Ethylene is another fuel that is widely available due to the production of plastics. Previous fuel cell studies have shown that ethane reacts much slower than ethylene in fuel cells [6]. The purpose of this chapter is to compute the energies required to remove the first and second hydrogen atoms from ethane absorbed on a nickel catalyst surface to create an ethylene molecule adsorbed on the catalyst surface and determined whether or not the energy needed for either of these hydrogen removal reactions can be attributed to the difference between the performance of ethylene and ethane fed fuel cells.

Density Functional Theory (DFT) is a method that uses electron density to determine the ground state energy of a system of molecules [7]. Siesta uses the probability of an electron being found in a given location to determine the energy of the simulation system [8]. Since DFT can predict the ground state energies of simulation systems, the goal of this chapter is to use DFT to study the energetics of hydrogen-carbon bond breaking and relate them to the difference in performance of fuel cells operating with ethane and ethylene. This will allow some conclusions to be drawn on the effect of hydrogen-carbon bond breaking on fuel cell performance and whether it might be rate limiting in the electrochemical reaction. The dissociation of adsorbed hydrogen gas will also be studied as a comparison since it is the most widely understood fuel used in PEM fuel cells.

4.2. Computational Methodology

4.2.1. Density Functional Theory

Density Functional Theory (DFT) is a computational method that uses electron density to determine the ground state energy of a simulation system. It has gained popularity because the use of electron density limits the complexity of the calculation as compared to other approaches such as wave function methods. DFT is still limited by computational power [9]. More complex

simulation systems take more time to converge to the lowest energy state due to the additional atoms included in the more complex systems. There are many software packages available that perform DFT calculations and the one selected for use in this work was SIESTA [8].

4.2.2. SIESTA

SIESTA (Spanish Initiative for the Electronic Simulation of Thousands of Atoms) is the software package that was selected for ~~use to~~ perform DFT calculations. It does so through an iterative method where it slowly moves atoms in different directions in order to minimize the ground state energy of the system. It was selected due to its ability to perform electronic structure calculations while providing control of the time, or cost, of each simulation by tuning several different factors: cutoff points at which the simulation can be said to have converged, step sizes, the maximum number of step sizes, and the number of k-points in the system. This permitted faster simulations for exploratory work and more fine-tuned simulations for calculations of final system simulation energies [8].

SIESTA represents each atomic species in the form of a pseudopotential. The purpose of the pseudopotential is to replace the core electrons with a potential [10]. Then electronic calculations are only performed on valence electrons. This is beneficial as it decreases the number of electronic calculations and thereby lowers the cost of the simulation while retaining the relativistic effects of the core electrons. There are different software applications available to create the pseudopotential files and the one selected for use in this work was ATOM.

4.2.3. ATOM

ATOM is the software package that was used to generate pseudopotential files for each atomic species for use by SIESTA to perform DFT calculations. It prepares the electronic configurations of atomic species [10]. The following are specified: number of core orbitals, number of valence orbitals, and for each valence orbital the following are specified: principal quantum number, angular momentum quantum number, and number of electrons located in each valence orbital. Several pseudopotential generation schemes are available in the software. The

Troullier-Martins generation scheme was selected due to its simplicity compared to the other models.

ATOM also contains standard pseudopotential files and tests to compare the generated pseudopotential files to ones that are generally considered to be standard. This is done by simulating molecules and atoms with the generated pseudopotential files, followed by comparison with the standard ones. Deviations between energy states and final geometries are noted. These tests are beneficial in ensuring that the generated pseudopotential files lead to accurate simulation results.

4.2.4. Methodology

Once a pseudopotential file has been created for each species, an input file for SIESTA can be created to specify how the simulation should proceed. The input file is used to specify which model should be used to perform the calculation, the locations of the individual atoms in the initial geometry of the system, and the constraints that determine when a simulation has reached convergence.

The convergence technique which SIESTA uses to perform DFT calculations needs to be specified in the input file. There are several convergence techniques available for use. Both the Broyden and the Conjugate Gradient convergence techniques were tested. The ground state energy of the system would oscillate without converging when using the Broyden convergence technique. Therefore, the Conjugate Gradient model was used for all simulations. The Conjugate Gradient convergence technique does not converge as quickly as the Broyden one. Compensation for this can be achieved by an increase in step size between iterations.

The cutoff point at which the simulation can be considered converged can also be specified and so can the size of the steps between each iteration. The larger the values of these specifications, the faster the simulation will converge. However, large values can also sacrifice the accuracy of the convergence. The more complicated geometries had difficulty converging, so the step sizes were constrained beyond the default value by a factor of 10 to limit oscillations and to permit the simulations to converge. This increased both the number of steps and the amount of

time it took for the simulation system to converge, but it was necessary to reach a minimum energy.

The specification of the geometry of the unit cell and the location of individual atoms within the unit cell is also done in the input file. SIESTA uses repeating or periodic boundary conditions. If the unit cell is repeated in all three directions, a three dimensional solid is obtained. If the unit cell is repeated in only 2 directions a slab is formed. If the unit cell is not repeated at all a cluster is formed. Large amounts of vacuum are specified in the direction(s) that the unit cell should not be repeated. For example, specifying a large amount of vacuum in the z-direction will be interpreted as a slab calculation. SIESTA will then repeat the unit cell in the x- and y-directions. In the z-direction there will be a series of slabs each interspersed by a large amount of vacuum. Cluster calculations were used for individual molecules, while slab calculations were performed for any calculation involving a catalyst surface.

A bi-product of the unit cell size of and the slab size is the number of k-points in the simulation system. (k-points are sampling points in the first Brillouin zone.) The larger the unit cell, the more k-points there are in the system. The larger the slab size (the real-space cell) the smaller the reciprocal space and the fewer k-points needed. The number of k-points is a reflection of how fine the mesh is that SIESTA uses to perform its iterative calculations. Those simulations that have a larger number of k-points have a finer mesh. The number of k-points also affects the time required for each iteration in a ground state energy calculation. The more k-points in the system, the longer it takes to calculate each step. This increases the time it takes for the simulation to converge. However, having fewer k-points can lead to inaccurate results in the simulations. It is important to find a balance between time, or cost, and accuracy. 32 k-points were used in our simulations. With 32 k-points there was not much difference in ground state energy when the number of k-points was varied.

The positions of the individual atoms in the unit cell can be specified as fixed or relaxed. A fixed position is one that cannot move whereas a relaxed position is one that can be moved in order to minimize the energy of the system. Each coordinate of an atom needs to be specified as fixed or relaxed. This permits atoms to move in 3-dimensions, or on a plane, or along a line, or

not at all. Fixing atom positions can be useful in controlling the cost of a simulation. Each fixed atom means there is one less atom for which movement must be calculated. However, it does not reflect reality. In particular, the surface atoms of a catalyst are free to move in any direction. Similar to k-points, a balance needs to be found between cost and accuracy.

When optimizing molecules or atoms, the atoms are specified as relaxed in all directions to yield the optimal geometry. Simulating molecules or atoms is fast as the systems do not contain many atoms. This allows for the calculation to converge quickly even when all the atoms are relaxed in all directions. These calculations are useful as they give the ground state energy of the molecule or atom in the gas form.

After the molecules were optimized, the nickel catalyst slab was optimized. Due to the amount of nickel atoms in the slab, it was decided not to relax the nickel atoms and keep them at the same positions they have the crystalline structure of bulk nickel. This is not an accurate representation of surface ~~of~~ nickel atoms since they do not retain the bulk crystalline structure. However, this decision was made to simplify future adsorption runs and reduce the cost of each simulation. Allowing the nickel atoms to relax drastically increases the time the simulation takes to converge. Also, many more initial orientations of the substrate molecules on the surface of the catalyst are possible. The simulations of the nickel slab by itself gave the ground state energy of the catalyst slab.

To determine the initial adsorbed geometry of a system, one of the atoms in a molecule being adsorbed (eg. a carbon atom in ethylene) is positioned at a fixed distance from one of the nickel atoms in the nickel slab. The coordinates of the other atoms in the adsorbed molecule are relaxed. Subsequent calculations were performed by varying that fixed distance. The energy of the simulation system will vary as the fixed distance is varied. Gradually allowing the molecule to approach the catalyst surface, by changing the fixed distance, and determining which of the fixed distances provides the lowest ground state energy and yields the initial geometry of the adsorbed system prior to bond breaking.

This initial adsorbed geometry was then converted into spherical coordinates. This was important for bond breaking for two reasons: it allows for all the bond lengths to be controlled (fixed or relaxed), and it allows for the locations of all atoms to be relaxed while maintaining a particular bond length. SIESTA operates by decreasing the ground state energy of a system. By lengthening a bond, the energy of a system is increased. Fixing a bond length at the longer value permits the bond to be lengthened without SIESTA returning the adsorbed state of the molecule. Relaxing the locations of atoms permits the bond length to remain lengthened while SIESTA moves the atoms around to minimize the energy of the system. The energy values for the breaking of bonds was determined by gradually increasing a bond length until a maximum energy was calculated for the system.

4.3. Results and discussion

4.3.1. Study of Different Approaches to Bond Breaking

The purpose of this study is to investigate the energetics of the dehydrogenation of ethane to ethylene. This requires the removal of hydrogen atoms from ethane adsorbed on a catalyst surface one at a time to determine the ground state energy of intermediate species. These predicted ground state energies of intermediate species will help in the understanding of which steps in the oxidation reaction are rate limiting.

There are two different approaches that can be used to assess the energetics of an intermediate step. One method is to gradually stretch a given bond length until the energy goes through a maximum and then decreases to a constant value. The constant value is obtained when the bond is completely broken. The other method is to start with the final product molecule and gradually bring an atom toward it from afar until the energy goes through a maximum and then decreases to the energy of the initial adsorbed species. This second method is essentially plotting the same curve as the first method, just in the opposite direction. Both methods are used in this investigation.

Under different circumstances, one method may be more easily executed than the other. For instance, it is easy to gradually stretch a carbon-hydrogen bond in adsorbed ethane since the

initial geometry of the system is clearly defined. However, the structure of an adsorbed C_2H_5 radical on a catalyst surface may not be as clearly defined. For this case, it might be easier to gradually introduce a hydrogen atom to adsorbed ethylene on a catalyst surface since the final geometry of adsorbed ethylene is clearly defined.

4.3.1.1. Hydrogen Dissociation

Hydrogen gas is the most frequently used feedstock for fuel cells because it reacts rapidly. Therefore, hydrogen gas dissociation reaction was used as a comparison with the ethane dissociation reactions. The bond length of an adsorbed hydrogen gas molecule on a nickel catalyst bed was gradually stretched to see how the system energy changed. The geometries of the adsorbed hydrogen species and the transition state are visualized in Figure 4.1 below. It was compared it to the ground state energy of a system of adsorbed hydrogen on nickel. The differences in energies as a function of bond length can be seen in Figure 4.2 below.

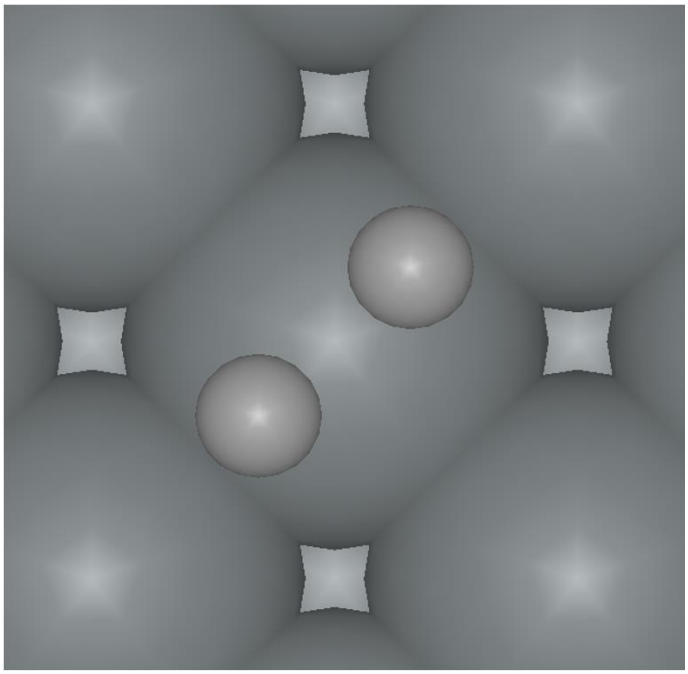

Figure 4.1: Hydrogen gas at the transition state in dissociation

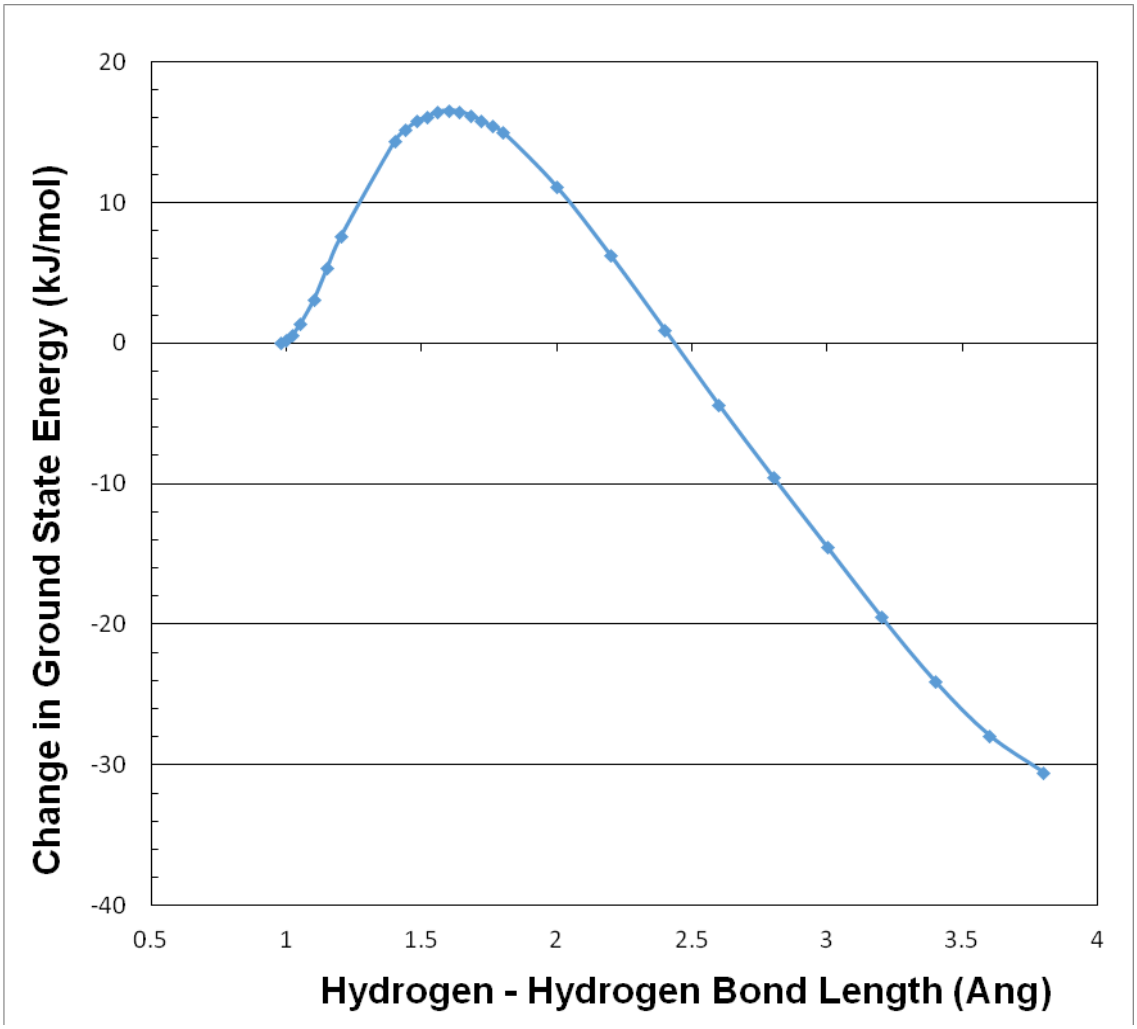

Figure 4.2: Ground state energy [kJ/mol] versus hydrogen – hydrogen bond length [Å]. Adsorbed hydrogen was arbitrarily assigned a ground state energy of 0 kJ.mol. The activation energy(the energy of the transition state), 16 kJ/mol, is the maximum energy value in the diagram

The maximum energy value in Figure 4.2, 16 kJ/mol, is the endothermic energy necessary for an adsorbed hydrogen molecule to reach its transition state. It is the activation energy to form the transition state for the hydrogen dissociation reaction. It should be noted that the activation energy, 16 kJ/mol, necessary to reach the transition state, is less than the energy released by the adsorption of hydrogen gas to form an adsorbed hydrogen molecule on a nickel catalyst (97 kJ/mol reported in the Adsorption Chapter). That means the adsorbed hydrogen molecule has sufficient energy to provide the activation energy for reaction without receiving

additional energy either from the vibrations of the nickel catalyst or from gas phase ethane molecules that collide with the adsorbed hydrogen molecule.

As the hydrogen bond length increases beyond the bond length at the transition state the energy of the system decreases. Eventually the energy of the system decreases below the energy of an adsorbed hydrogen molecule. That makes the net energy of reaction exothermic.

4.3.1.2. Removal of the First Hydrogen Atom from Ethane

The first step in the oxidation of ethane to ethylene is the removal of one of the hydrogen atoms. As the system geometry of adsorbed ethane is well understood, the approach taken was to gradually stretch one of the C–H bonds while allowing the system to relax to a new geometry. There are six hydrogen atoms that can be selected for removal. The one selected, circled in Figure 4.3 below, was arbitrarily chosen to be the one to be removed.

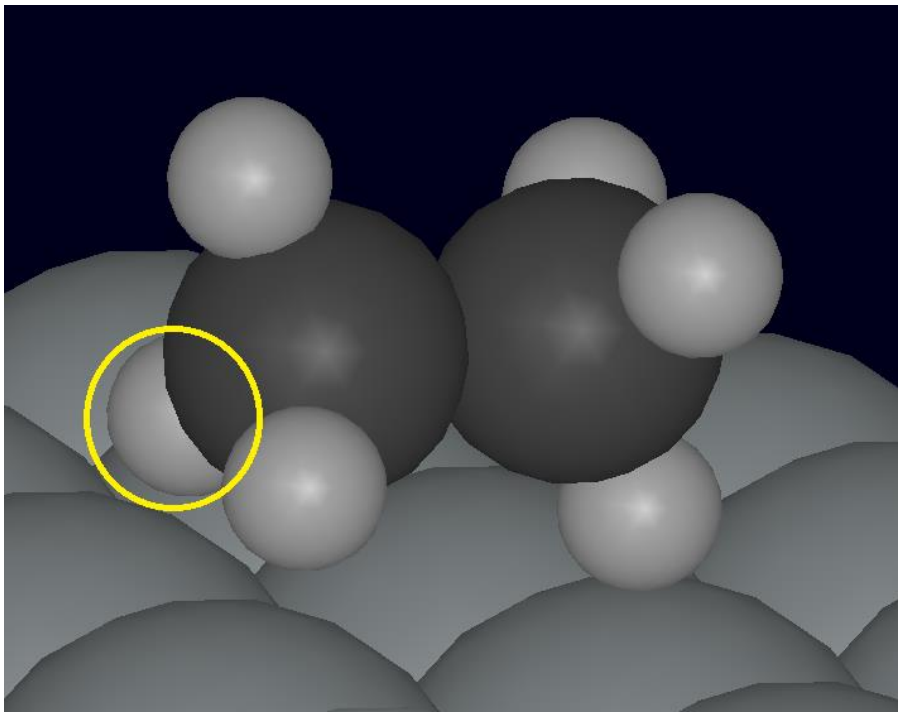

Figure 4.3: Visualization of an ethane molecule on the surface of a nickel slab. The first hydrogen to be removed from ethane is identified by the circle on the left side.

The hydrogen circled in Figure 4.2 is one of the three hydrogen atoms located near the catalyst surface. Therefore it can easily interact with the nickel atoms. The bond length between this hydrogen atom and its carbon atom was increased. The resulting variations in the energies of the system are shown in Figure 4.4 below as a function of carbon-hydrogen bond length.

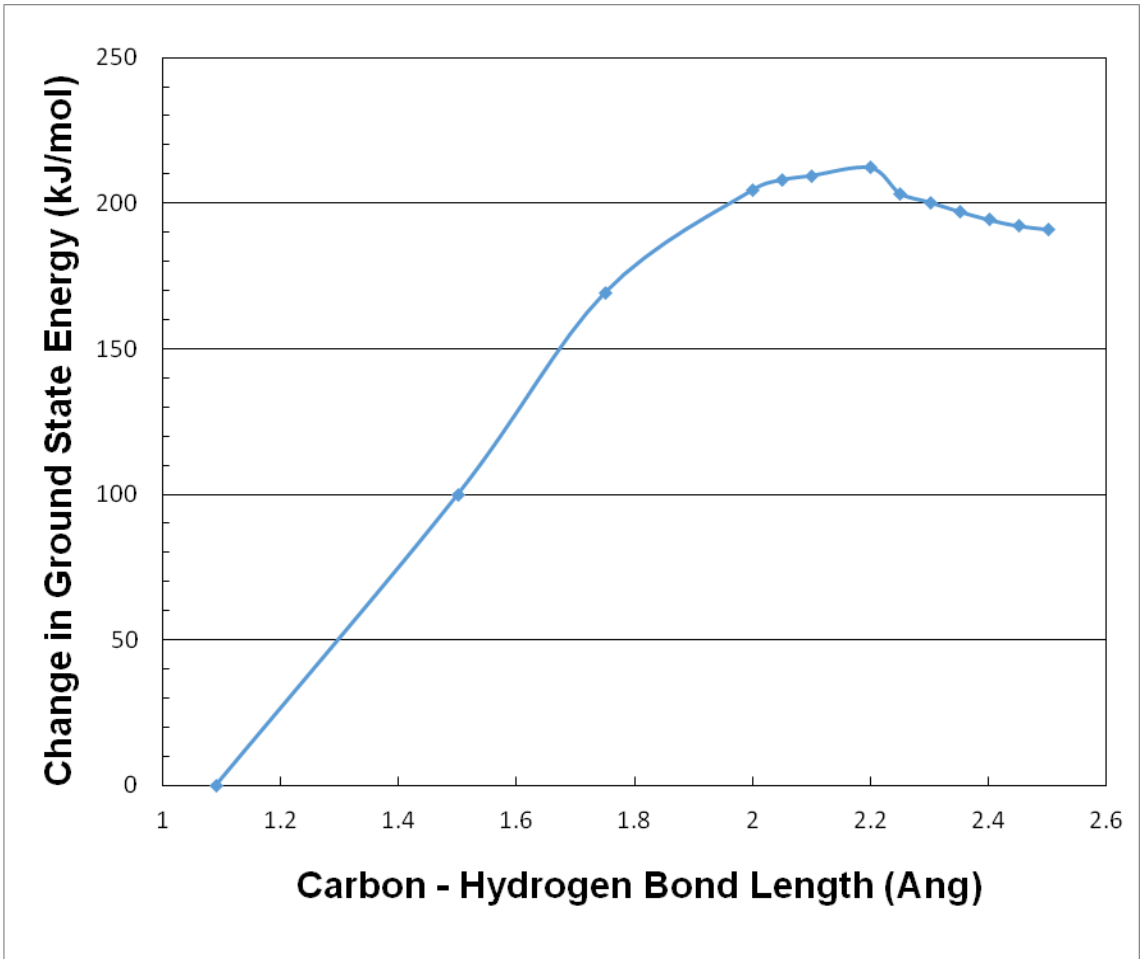

Figure 4.4: Ground state energy [kJ/mol] versus carbon – hydrogen distance [Å], as the first hydrogen is removed from adsorbed ethane. Adsorbed ethane was arbitrarily assigned a ground state energy of 0 kJ/mol. The activation energy (the energy of the transition state), 210 kJ/mol, is the maximum energy value in the diagram

From the predicted energy values in Figure 3, it appears that the removal of the first hydrogen atom from an adsorbed ethane molecule requires an activation energy of approximately 210 kJ/mol of energy (endothermic). That value is 3 times larger than the energy that is released in the adsorption of ethane of 69 kJ/mol (exothermic) as reported in the Adsorption Chapter. The

energy of this transition state has a value above the ground state energy of adsorbed ethane. Therefore this step in the oxidation of ethane to ethylene is endothermic.

Some insight is gained by comparing the ratio of adsorption energy of a molecule to the activation energy for bond breaking. For hydrogen 97 kJ/mol are provided during adsorption and an activation energy of 16 kJ/mol is required to form the transition state in order to break the H–H bond. In comparison, for ethane 69 kJ/mol are provided during adsorption and an activation energy of 210 kJ/mol is required to break the C–H bond. When the ratio is greater than 1 (97/16 for hydrogen), a molecule has sufficient energy to provide the activation energy for reaction without receiving additional energy either from the vibrations of the nickel catalyst or from gas phase ethane molecules that collide with the adsorbed hydrogen molecule. When it is less than 1 (69/210 for ethane) energy transfer is required to provide the activation energy to form the transition state.

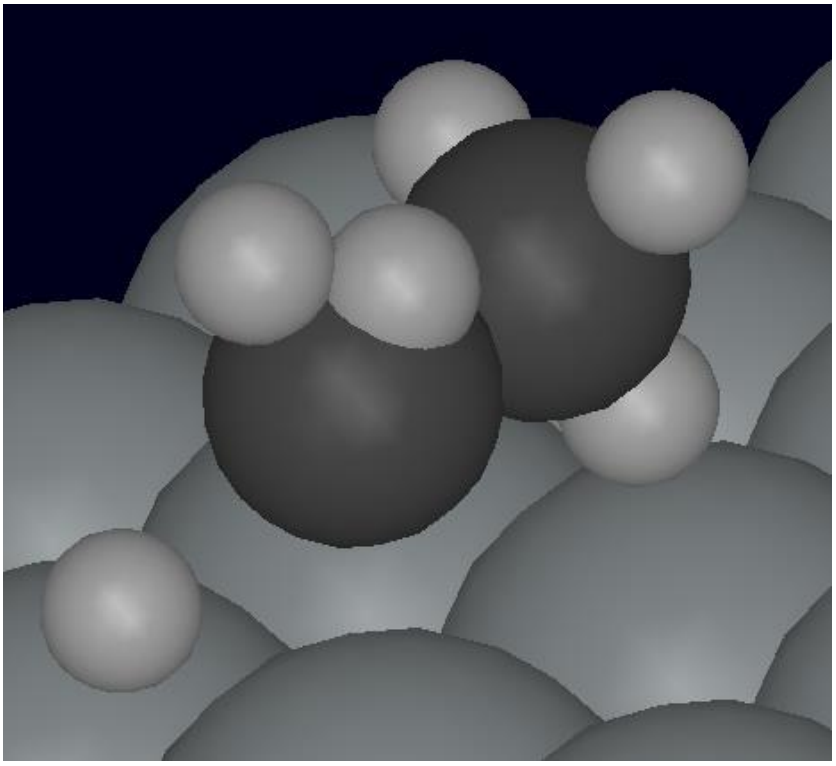

Figure 4.5: Geometry of the ethyl radical transition state when a hydrogen atom is removed from ethane.

The geometry of the system at the transition state is shown in Figure 4.5. Being able to visualize the geometry of a transition state is one of the powerful attributes of computational research. Species in a transition state are unstable. When compared to the geometry of stable molecules, it is reasonable to expect transition state geometries to be weird and unusual. The geometry in Figure 4.4 would definitely not be expected in a stable molecule. For gas phase ethane molecules charge is transferred from the carbon atoms to the hydrogen atoms. For the ethyl radical in Figure 4.4, it will be seen later (Figures 4.10 and 4.11) that additional charge is transferred from the nickel catalyst atoms to the carbon atom in Figure 4 having the two attached hydrogen atoms. Undoubtedly the charge transfer from the catalyst contributes to the weird and unusual geometry seen in Figure 4.5.

4.3.1.3. Removal of the Second Hydrogen Atom to form Ethylene

The second step in the oxidation reaction of ethane to ethylene is the removal of a second hydrogen atom from the original ethane molecule that became an ethyl radical. The calculations were started using adsorbed ethylene, because its structure was known with a high degree of certainty. Then a hydrogen atom was added to the adsorbed ethylene to form the ethyl radical.

The hydrogen atom from afar was gradually placed at positions closer and closer to an adsorbed ethylene molecule. This is essentially plotting the same curve for energy versus C–H distance, but in the opposite direction. The hydrogen atom to be added was initially located at a distance slightly less than 2.1 Angstroms from one of the carbon atoms in the ethylene molecule adsorbed on the nickel catalyst. Subsequently the distance between the hydrogen atom and the carbon atom in the ethylene molecule was gradually decreased.

As the carbon – hydrogen bond distance decreased, the energy went through a maximum, as shown in Figure 4.. The energy was virtually invariant as the bond length changed from 1.2 Å to 1.09 Å, the carbon – hydrogen bond length in ethylene. The bond length between the carbon atom and the hydrogen atom added to form the C_2H_5 transition state (approximately 1.3 Å in Figure 4.5) is greater than C–H bonds in either in adsorbed ethane (1.1 Å in Figure 4.3) or in adsorbed ethylene (1.09 Å in ethylene in Figure 4.5). The longer C–H bond length in the transition state is one indication that the C_2H_5 transition state is in an unstable species.

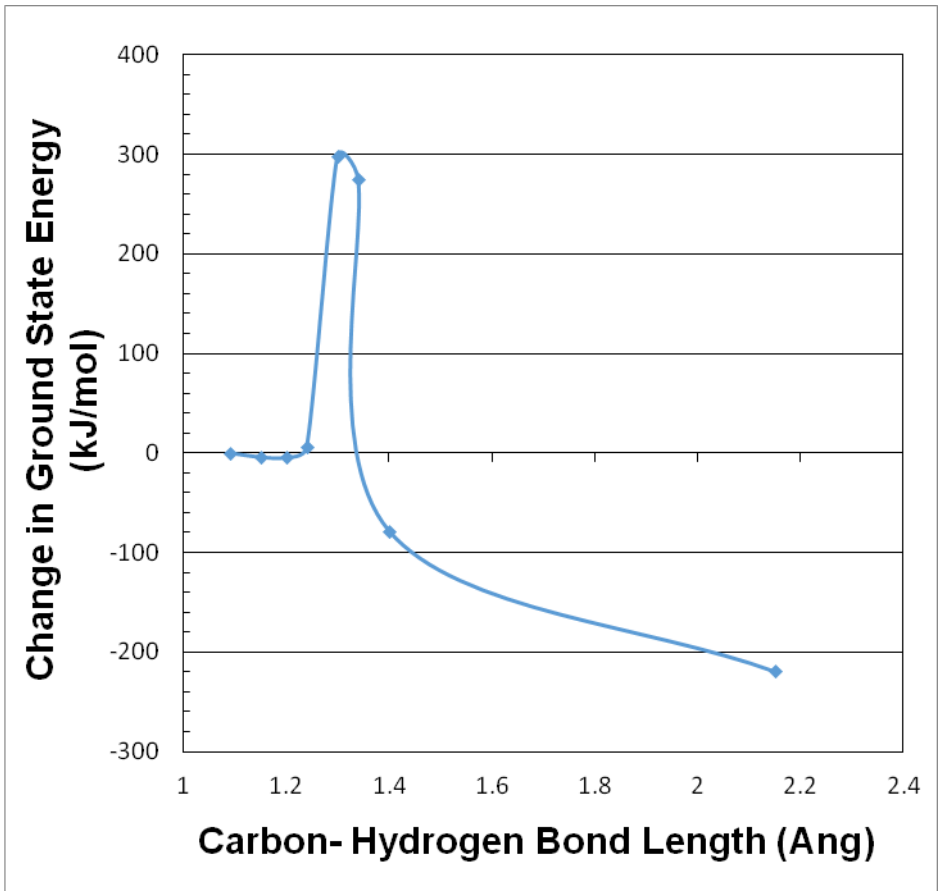

Figure 4.6: Ground state energy versus carbon – hydrogen distance, as a hydrogen atom is added to the adsorbed ethylene. Adsorbed ethylene was arbitrarily assigned a ground state energy of 0 kJ/mol. The activation energy (the energy of the transition state), 300 kJ/mol, is the energy difference between the energy of the adsorbed ethyl radical whose C-H distance is 2.2 Å and the maximum energy.

From the predicted energy values, it appears that the removal of the second hydrogen atom from an adsorbed ethane molecule requires an activation energy of approximately 300 kJ/mol. In comparison, this value is larger than the energy that is released during the adsorption of ethylene of 214 kJ/mol as discussed in the Adsorption Chapter. Therefore the ratio of adsorption energy to activation energy, 214/300, is less than 1.

Reaction kinetics follow the Arrhenius law, $k = A \exp(- E_A/RT)$. If the pre-exponential factors, A, are similar, then the activation energy values, E_A, would be expected to determine the

rate constant, k. Since removal of the second hydrogen atom has the greatest activation energy, it would be the rate-limiting step. Surface processes (reaction kinetics or adsorption kinetics) known as "activation" processes in the fuel cell literature are generally accepted to be rate limiting at small current densities for fuel cells that use hydrogen as the fuel.

Reaction kinetics for ethane can be compared with those for hydrogen, assuming the pre-exponential factors are similar. The activation energy for H–H bond breaking is 16 kJ/mol. The activation energies for C–H bond breaking are 210 and 300 kJ/mol. That comparison indicates that the reaction with hydrogen would be faster. Since the fuel cell reaction with hydrogen is known to be faster than with ethane, it can be concluded that these calculations are consistent with experimental observations.

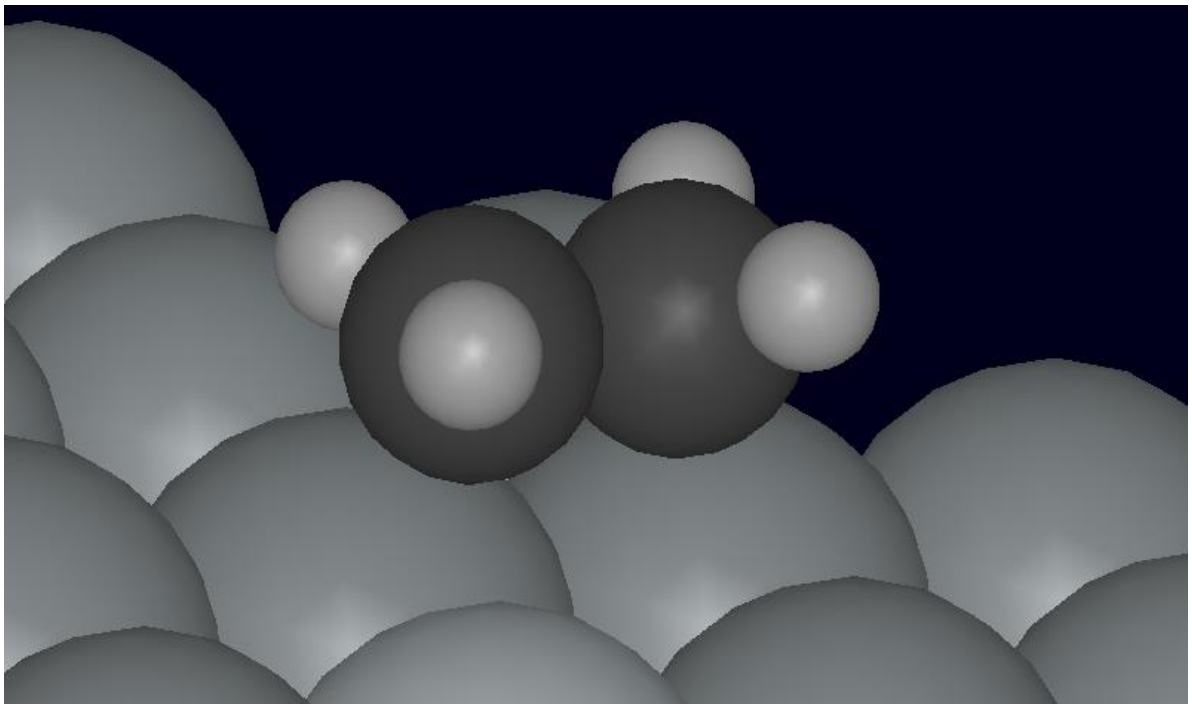

Figure 4.7: Final geometry of the transition state when the second hydrogen is removed from ethane.

The final geometry of the transition state when a hydrogen atom is being added to adsorbed ethylene is shown in Figure 4.7. The view of the transition state in Figure 4.6 is puzzling because the hydrogen atom added to the ethylene does not appear in Figure 4.7.

However, when the nickel atoms underneath the transition state radical are removed from the figure the hydrogen atom becomes visible as shown in Figure 8.

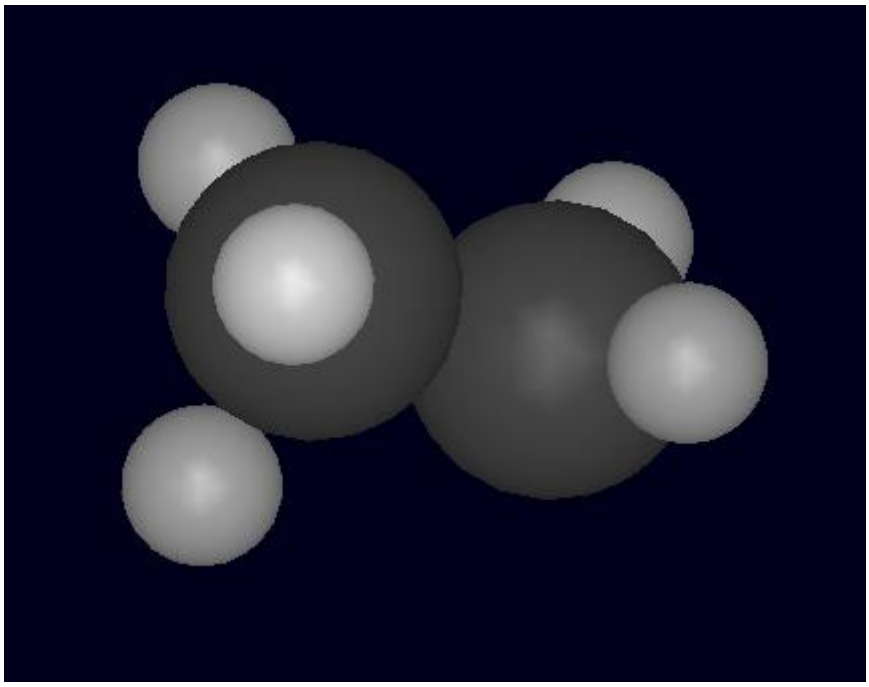

Figure 4.8: Final geometry of the C_2H_5 transition state compared to that in Figure 4.7. The difference is the visibility of the 5th hydrogen atom

The visualization software has an influence on the appearance of the transition state geometry shown in Figures 4.7 and 4.8. The visualization software uses standard atomic diameters that have a different value that is constant for each element of the periodic table. Unfortunately they do not vary with bond distance between atoms. The four hydrogen atoms originally attached to the carbon atoms in the original adsorbed ethylene molecule did not move much and the two carbon atoms stayed in the same plane. Therefore invariant atomic diameters do not affect the appearance of those atoms. The C–H bond for the hydrogen atom that was missing from Figure 7 was 1.3 Å as indicated in Figure 4.6. In Figure 4.7 the Ni atom appears to touch the carbon atom. As a result there must have been a very short H–Ni bond involving the hydrogen atom that was missing from Figure 4.7. The H–Ni bond must have been sufficiently short so that the entire standard hydrogen atomic diameter would have been located within the standard Ni atomic diameter. Again computational research has made possible the visualization of another weird and unusual geometry for a transition state.

4.3.2. Mulliken Population Analysis

4.3.2.1. Hydrogen Dissociation

A Mulliken Population Analysis was performed in order to calculate the charges transferred between an adsorbed hydrogen molecule and a nickel catalyst slab when a hydrogen molecule dissociates into two adsorbed hydrogen atoms. When a hydrogen molecule is adsorbed onto a nickel slab, 9 nickel atoms share their charges with the hydrogen molecule. In Figure 4.9 these are seen to be the nickel atom that the hydrogen molecule adsorbs onto (change in charge + 30) and the 4 nickel nearest neighbour atoms adjacent to this nickel atom (change in charges –24, –39, – 46) and the 4 next nearest neighbor nickel atoms (change in charge +12). The change in charge is the charge difference between the adsorbed state and the transition state. When the change in charge is negative, the nickel atom has lost charge. When the change in charge is positive, the nickel atom has gained charge. With one exception, charges in charge are lost from the nickel atoms and are taken up by the two hydrogen atoms.

These changes from bare Ni slab to adsorbed H_2 molecule are shown in Figure 9 below. The adsorption site is indicated by the numbers written in red with differences multiplied by a factor of 1000. The H_2 molecule is centered over the atom that says + 30 in the middle and the two hydrogen atoms are closest to the atoms that have charges of - 46 and -39.

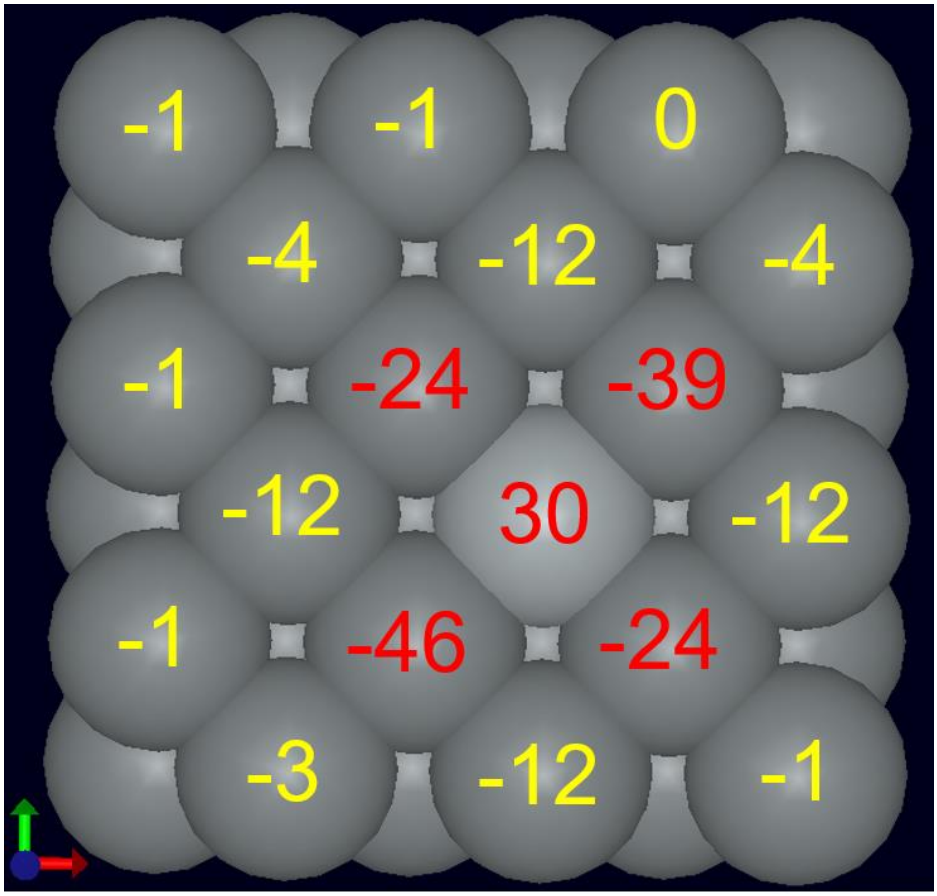

Figure 4.9: Change in charge distribution on each atom in the nickel catalyst slab between the adsorbed state and the transition state in hydrogen dissociation

The atom directly under the adsorbed hydrogen molecule (indicated by the + 30) has gained charge while the others have lost. This indicates that as the hydrogen atoms move apart from each other and closer to the adjacent nickel atoms, the adjacent nickel atoms begin to contribute more charge to the hydrogen atoms. It can be concluded that to investigate hydrogen dissociation reactions, it is important to have a fairly large unit cell. A minimum of 9 nickel atoms in the unit cell would be needed to achieve these results and less would interfere with how the charges are shared through the system.

4.3.2.2. Removal of the First Hydrogen from Ethane

A Mulliken Population Analysis was performed in order to calculate the charges transferred between an adsorbed ethane molecule and a nickel catalyst slab change when one of the hydrogen atoms is removed from the ethane molecule. Chapter 3 showed an ethane molecule adsorbed onto a nickel slab.

4 nickel atoms shared their charges with the ethane molecule. Those four Ni atoms with charges are the ones that have the blue colour in Figure 4.9. Two of the nickel atoms in Chapter 3 are located directly under carbon atoms of the ethane molecule. The other two nickel atoms are adjacent to the carbon atom that has two hydrogen atoms. In the adsorbed state (Chapter 3), charges are lost from the nickel atoms and are taken up by the two carbon atoms and the 3 hydrogen atoms that face the nickel slab in Chapter 3.

However in Figure 4.10 (here in Chapter 4), once one of the hydrogen atoms has been removed from the adsorbed state to form the transition state, it appears that there is a shift in charge sharing. The changes in charge distribution in the nickel catalyst slab are summarized in 4.10 below. The original site of adsorption is shaded in blue. All differences in charges are multiplied by a factor of 1000. The corresponding changes in charges on the carbon and hydrogen atoms in the transition state are shown in Figure 4.11.

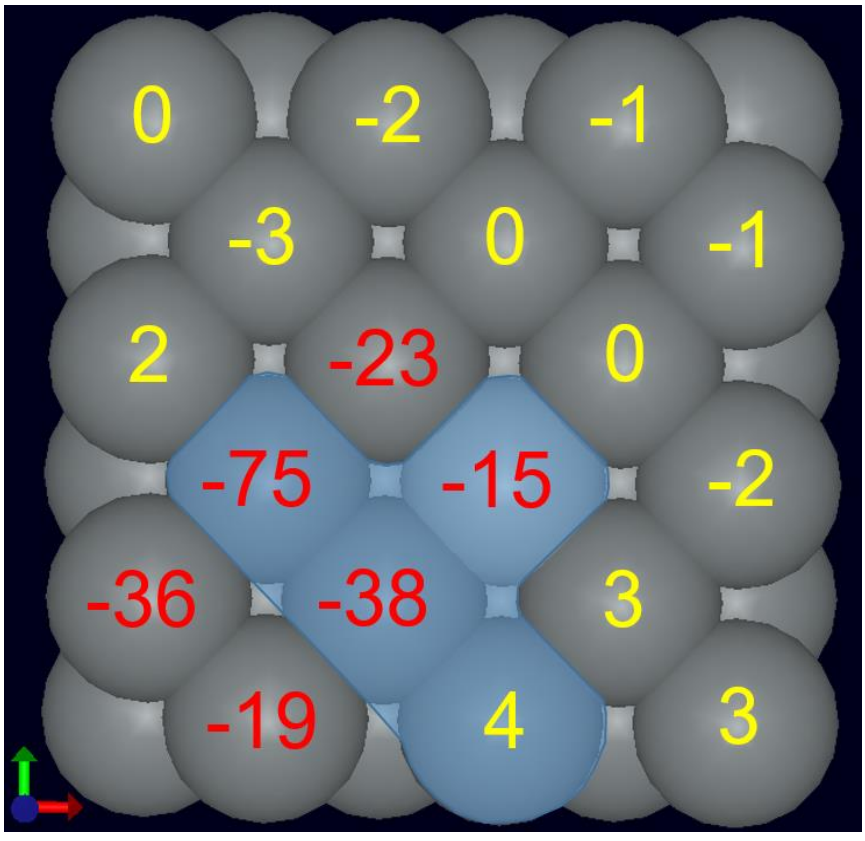

Figure 4.10: Change in charge distribution in a nickel catalyst slab when an ethane molecule adsorbed on a nickel slab is converted into the transition state for the transformation that occurs as the first hydrogen is removed from the ethane.

It appears the reaction site for the transition state is composed of 6 nickel atoms rather than the four nickel atoms used in the adsorption site. The charge transferred from the nickel atoms has also increased. Most of the additional charge from the nickel atoms has been transferred to the carbon in the transition state, shown in Figure 4.11, that has two attached hydrogen atoms. Again, all charges are multiplied by a factor of 1000.

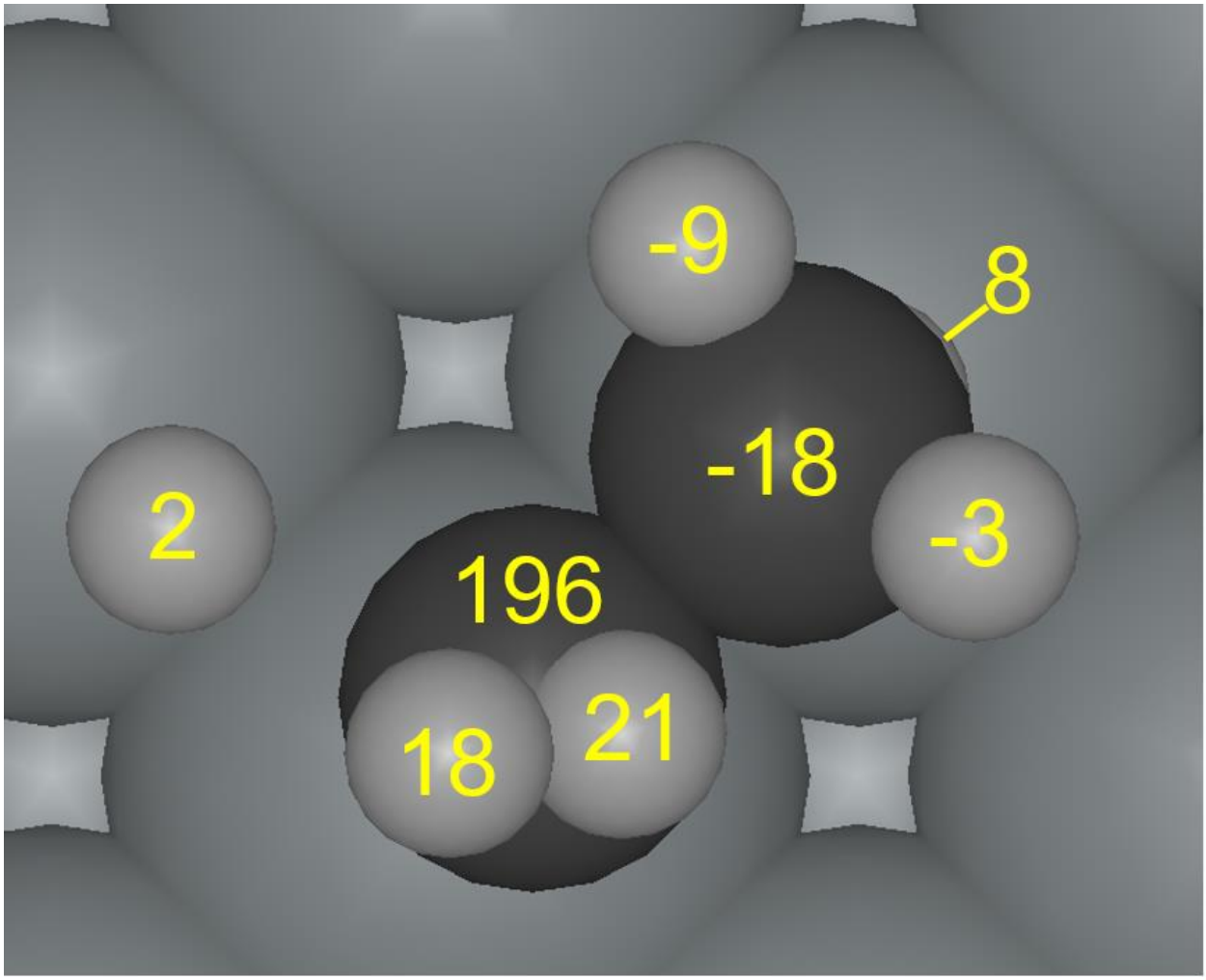

Figure 4.11: Change in the Charge Distribution in the hydrocarbon species during the transformation of an adsorbed ethane molecule to the transition state formed as the first hydrogen is removed

4.3.2.3. Removal of the Second Hydrogen to form Ethylene

Transition states are unstable and high energy. In this case the structure of the transition state is quite different than the stable ethylene molecule. The total charge number of the transition state is similar to that of the sum of the gas phase ethylene molecule and that of a gas phase hydrogen atom. The charge of the hydrogen atoms in C_2H_5 are similar to those in ethylene (with the exception of the H atom being added).

There were significant changes to the charge numbers on the two carbon atoms. The carbon atom (-357) with 3 hydrogen atoms has become much more charge deficient. Some of that charge has gone to the third hydrogen atom (+135) and some of the charge has gone to the carbon atom (+253) with two hydrogen atoms. The result is that the C_2H_5 species can be described as a dipole. It is not surprising that the C_2H_5 species is a dipole since one of the carbon atoms has 3 hydrogen atoms and the other carbon atom has 2 hydrogen atoms.

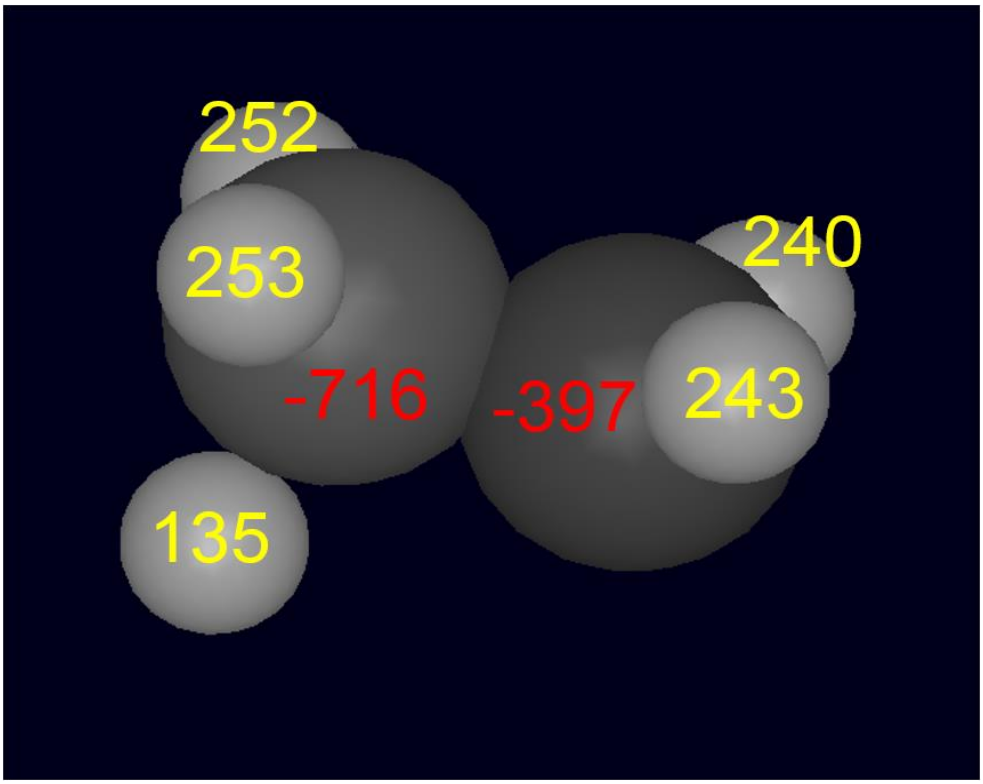

Figure 4.12: Changes in charge numbers between the C_2H_5 transition state compared to the C_2H_4 molecule in the gas phase. All numbers are multiplied by 1000

The two nickel atoms underneath the two carbon atoms have charge numbers that are the reverse of the change in charge numbers of the two carbon atoms. The 2 nickel atoms have formed a reverse dipole ~~to~~ that mirrors the dipole in the C_2H_5 species. This dipole in the nickel catalyst slab can be seen in Figure 4.13. The nickel atom with a charge number of +75 is the nickel atom situated under the carbon atom (-357) with 3 hydrogen atoms attached to it. The nickel atom with a charge number of -116 is the nickel atom situated under the carbon atom (+253) with 2 hydrogen atoms attached to it.

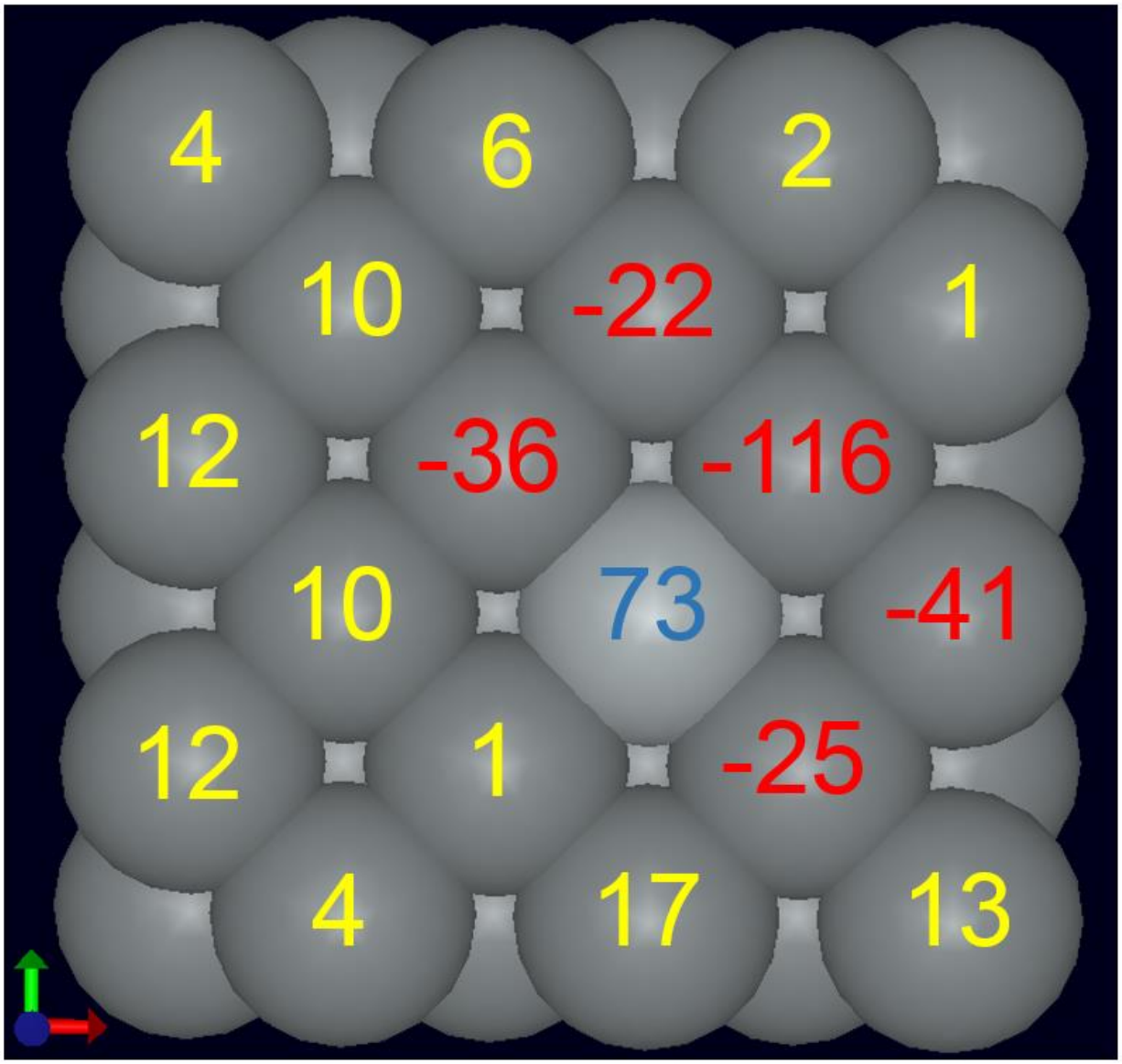

Figure 4.13: Charge numbers in the nickel catalyst slab under the C_2H_5 radical in the transition state. All numbers are multiplied by 1000.

4.4. Conclusions

In terms of energy, hydrogen gas readily dissociates when adsorbed by a nickel catalyst, requiring approximately 16 kJ/mol of activation energy to reach the transition state, in contrast to the 97 kJ/mol made available during adsorption. The overall dissociation reaction is exothermic. This helps explain why hydrogen gas appears to work well in fuel cells using hydrogen as a fuel source.

The removal of the first hydrogen from ethane was predicted to require 210 kJ/mol to reach the transition state. The difference in energy, in Figure 4, between the reactant species and the product species show it is an overall endothermic process. The removal of the second hydrogen from ethane is the step that requires the most energy at 300 kJ/mol, to reach its transition state. In Figure 6 it is seen that the transformation from the C_2H_5 species to the transition state and then to the final adsorbed ethylene product is exothermic. Adsorption processes do not have activation energies, whereas the bond breaking hydrogen removal reactions do have activation energies. As a result the bond breaking reactions are the rate limiting processes, rather than the adsorption processes.

Regardless of the size of the reacting species (H_2, C_2H_4, C_2H_6) on the catalyst surface, all nickel atoms directly underneath and adjacent to the atoms in the reacting species on the surface of the slab appear to play a role in the distribution of charges. Therefore, unit cells with a relatively large number of surface atoms should be used to avoid charge distribution interference between the reaction species in neighbouring slabs.

4.5. References

[1] H. A. Liebhafsky & L. W. Niedrach; "Fuel cells"; *Journal of The Franklin Institute*; vol. 269; no. 4; pp. 257-267; 1960.

[2] M. Winter & R. J. Brodd; “What are Batteries, Fuel Cells, and Supercapacitors?”; *Chem. Rev.;* 104; pp. 4245-4270; 2004.

[3] R. O'Hayre et al.; "Introduction"; *Fuel Cell Fundamentals*; 3rd Edition; Wiley; USA; pp. 3-24; 2016

[4] M. L. Perry & T. F. Fuller; "A historical perspective of fuel cell technology in the 20th century"; *Journal of The Electrochemical Society*; vol. 149; no. 7; pp. S59-S67; 2002

[5] A. Demirbas; "Future hydrogen economy and policy"; *Energy Sources, Part B: Economics, Planning, and Policy*; 12:2; pp. 172-181; 2017

[6] E.J. Cairn & D.I. Macdonald; *Electrochemical Technology 2*; 65-70; 1964

[7] W. Kohn; "Overview of Density Functional Theory"; *Density Functional Theory*; edited by E. K. U. Gross and R. M. Dreizler; Springer Science+Business Media; USA; pp. 3-10; 1995

[8] E. Artacho et al.; "SIESTA 2.0.2"; Fundacion General University; Spain; 2008 (http://www.uam.es/siesta)

[9] N. Schuch & F. Verstraete; "Computational complexity of interacting electrons and fundamental limitations of density functional theory"; *Nature Physics*; Vol. 5; pp. 732-735; 2009

[10] A. Garcia; "Atom User Manual"; University of Pais Vasco; Spain; 2006 (http://nf.nci.org.au/facilities/software/Siesta/2.0/atom.pdf)

[11] Y. Zhu, T. Robinson, A. Al-Othman, A. Y. Tremblay, & M. Ternan; "n-Hexane fuel for a phosphoric acid direct hydrocarbon fuel cell"; *Journal of Fuel*; Vol. 2015

CHAPTER 5

THE LINK BETWEEN ADSORPTION AND BOND DISSOCIATION

5.1 Overview

Both adsorption and bond dissociation happen in the oxidation reaction of ethane to ethylene. Both phenomena need to be calculated to create a complete picture of the energetics of the reaction. Both phenomena gave insight to how the reaction propagates.

5.2 Summary

Several phenomena were studied. The baseline studies involved the slab thickness, the slab surface area, and the orientation of the molecule on the slab. Subsequently, adsorption steps were investigated for hydrogen gas, ethane gas, and ethylene gas. Finally, transition states were from the adsorbed species to intermediates to the final product were investigated.

As a molecule approaches the surface the system energy decreases. It goes through a minimum. The system energy was studied as a function of distance between the molecule in the slab. Finally, the energy increases as the distance between the molecule and the nickel catalyst slab diminishes.

The slab surface area, the slab thickness and the orientation of a molecule on the slab were all studied using an ethylene molecule. Three different geometries of the ethylene molecule on the nickel catalyst slab were investigated. When the double bond of the ethylene molecule is

located over a valley between two adjacent nickel atoms the largest heat of adsorption was observed.

Slab areas consisting of 2, 4, 8, 18, and 32 nickel atoms were investigated. All of the slabs with 8 or more surface nickel atoms had the same heat of adsorption. Smaller surface areas correspond to greater surface coverages of ethylene and had greater heats of adsorption than the large slab areas.

The number of layers in a slab was investigated using slabs having 18 surface nickel atoms. The heat of adsorption was much higher on a single layer slab than on multi-layer slabs. As a result, slabs with two layers were used since the heats of adsorption on 2-layer slabs were not significantly different than the heats of adsorption on 3- and 4-layer slabs. By using slabs with 18 surface nickel atoms and two layers it was possible to calculate heats of adsorption that were not influenced by crowding from other ethylene molecules.

A system consisting of an adsorbed species on a nickel slab was compared to a system of the bare catalyst slab and a molecule in the gas phase to determine the heat of adsorption. For bond dissociation, the initial system was the adsorbed state. From the adsorbed state, a bond length was increased until a maximum was observed to determine the activation energy.

Four (4) steps of the oxidation reaction of ethane to ethylene in a nickel catalyt fuel cell were studied: the adsorption of ethane onto the surface, the removal of the first hydrogen from ethane, the removal of the second hydrogen from ethane, and the desorption of ethylene from the surface (opposite of adsorption). The adsorption of ethane onto the catalyst surface released 69 kJ/mol of energy. The removal of the first and second hydrogen atoms required 210 kJ/mol and 300 kJ/mol respectively. The desorption of ethylene from the surface required 214 kJ/mol. Clearly substantially more energy is required by dehydrogenation and desorption than is produced by adsorption. Based on the energy requirements for these four steps, it was concluded that the removal of the second hydrogen from ethane is the rate-limiting step.

Transition states are known to be unstable. The transition states for the two reactions that remove hydrogen atoms have large activation energies. These transition states required much larger flows of charge from the nickel catalyst slab than the adsorbed states required from the nickel catalyst slab. The weird geometries that were observed are consistent with the other three factors.

There were two steps of the hydrogen dissociation reaction in a nickel catalyst fuel cell that were studied: the adsorption of hydrogen gas onto the nickel catalyst surface, and the dissociation of the adsorbed hydrogen gas molecule into two adsorbed hydrogen atoms. The adsorption of hydrogen gas onto the catalyst surface released 96 kJ/mol of energy. The dissociation reaction required 16 kJ/mol. It is apparent that the adsorption of hydrogen gas onto the catalyst surface releases enough energy to meet the energy requirements for the dissociation of hydrogen and the molecule falls apart. This supports why hydrogen is the most popular cell fuel source.

5.3 Conclusions

Both surface adsorption and bond dissociation occur in the oxidation reaction of ethane to ethylene. Energy for both phenomena needed to be calculated to create a complete picture of the energetics of the oxidation reaction. However, there is one key link between the two parts of the oxidation reaction when using density functional theory: the final geometry of the adsorption calculation provides the initial geometry of the species that is used for the bond dissociation calculation. Without first doing adsorption, the starting point for bond dissociation is unknown.

Activation energy for hydrogen dissociation requires 16 kJ/mol of energy. The heat of adsorption of hydrogen gas is 96 kJ/mol. Therefore the heat of adsorption exceeds the activation energy required to form the transition state. Since no additional external is required to supply the activation energy, the hydrogen molecule virtually falls apart.

The removal of the first hydrogen from ethane had an activation energy of 210 kJ/mol. The removal of the second hydrogen from ethane had an activation energy of 300 kJ/mol. These two values are an order of magnitude higher than the activation energy of hydrogen gas

dissociation. Therefore, the removal of the second hydrogen is the rate limiting step. The requirement to provide the activation energies for the removal of these two hydrogen atoms from ethane (to form ethylene) is the factor that causes the reaction rate (current density) in an ethane fuel cell to be less than that in an ethylene fuel cell

Transition states are considered to be highly unstable. Compared to gas phase molecules, the transition states had excessively large charges and unusual geometries, which could be consistent with instability. Additionally, the Mulliken Analysis showed that the differences in charge distribution were larger in transition states than in adsorbed species.

This work shows that an appropriate unit cell size for the slab is larger than the unit cell sizes often used for slabs in literature.

5.4 Future Work

The objective of this study was to explore the reason(s) why fuel cells have higher current densities when ethylene is used as a fuel source as compared to ethane. The mechanism of the partial oxidation of ethane in a fuel cell results in ethylene as the product of a step. The remainder of the reaction is no different than that for the complete oxidation of ethylene. To determine why ethane performs poorly as a fuel compared to ethylene, only the step from ethane to ethylene needed to be studied. This study determined which step was rate limiting. Since this was the objective, no further work is proposed.

CHAPTER 6

CONTRIBUTION TO KNOWLEDGE

1. This work has provided new insight into the geometry of the adsorption sites occupied by ethane, ethylene, and hydrogen molecules. For example, there is a notion that an ethylene molecule might adsorb by breaking one of its two carbon–carbon bonds and using the electrons in that bond to form two bonds, each of which is between a carbon atom (in ethylene) and a nickel atom. In contrast the adsorption studies performed here showed that six Ni atoms are required for the ethylene adsorption site. This work also showed that four Ni atoms are required for the ethane adsorption site and that five Ni atoms are required for the hydrogen adsorption site.

2. This work has provided a new explanation for why hydrocarbon fuels react slower than hydrogen fuel in fuel cells. The ratio "exothermic heat of adsorption / endothermic activation energy" is calculated. For hydrogen the ratio was 95 kJ/mol / 16 kJ/mol = 5.94. The ratios for ethane and ethylene could be added here. When the ratio is greater than 1 the heat needed for the activation energy can be provided at the reaction site without the need for heat transfer from another location. When the ratio is less than 1 the rate of reaction may be limited by the rate of heat transfer from some other location (eg. the cathode) the energy of dissociation of adsorbed hydrogen if less than the heat of adsorption. This means that the energy released in adsorption (95 kJ/mol) is enough to cause the hydrogen molecule to dissociate into two hydrogen atoms as this process requires 16 kJ/mol. This may help explain why hydrogen gas reacts well electrochemically in fuel cells.